EFFECTS OF SUBSTRATE BIAS ON THE PROPERTIES OF a-Si:H FILMS FABRICATED BY ECR MICROWAVE PLASMA CVD

by

Thomas Yu-chau Tse

A thesis
presented to the University of Manitoba
in partial fulfillment of the
requirements for the degree of
Master of Science
in
Electrical Engineering

Winnipeg, Manitoba, 1988

(c) Thomas Yu-chau Tse, 1988

Permission has been granted to the National Library of Canada to microfilm this thesis and to lend or sell copies of the film.

The author (copyright owner) has reserved other publication rights, and neither the thesis nor extensive extracts from it may be printed or otherwise reproduced without his/her written permission.

L'autorisation a été accordée à la Bibliothèque nationale du Canada de microfilmer cette thèse et de prêter ou de vendre des exemplaires du film.

L'auteur (titulaire du droit d'auteur) se réserve les autres droits de publication; ni la thèse ni de longs extraits de celle-ci ne doivent être imprimés ou autrement reproduits sans son autorisation écrite.

ISBN 0-315-47989-2

EFFECTS OF SUBSTRATE BIAS ON THE PROPERTIES OF a-Si:H FILMS FABRICATED BY ECR MICROWAVE PLASMA CVD

BY

THOMAS YU-CHAU TSE

A thesis submitted to the Faculty of Graduate Studies of
the University of Manitoba in partial fulfillment of the requirements
of the degree of

MASTER OF SCIENCE

© 1988

Permission has been granted to the LIBRARY OF THE UNIVERSITY OF MANITOBA to lend or sell copies of this thesis, to the NATIONAL LIBRARY OF CANADA to microfilm this thesis and to lend or sell copies of the film, and UNIVERSITY MICROFILMS to publish an abstract of this thesis.

The author reserves other publication rights, and neither the thesis nor extensive extracts from it may be printed or otherwise reproduced without the author's written permission.

ABSTRACT

The optical, electrical and structural properties of a-Si:H films deposited by ECR microwave plasma CVD have been studied as functions of substrate bias and orientation with respect to the magnetic field. Films deposited on stainless steel substrates with their surfaces normal to the dc magnetic field exhibited good optical and electrical properties whilst films deposited on glass substrates with their surfaces parallel to the magnetic field exhibited poor optical and electrical properties. For moderate negative table bias, both films deposited on stainless steel and glass substrates exhibited higher density and better optical and electrical properties. These properties are explained in terms of ion bombardment and electron flow on the growing films.

ACKNOWLEDGMENTS

The author would like to thank Dr. K. C. Kao for his constant encouragement, advice and supervision throughout the course of this thesis.

Special thanks are due to everyone of the Materials & Devices Research Laboratory, in particular, T. T. Chau, T. V. Herak, S. R. Mejia, J. J. Schellenberg, P. K. Shufflebotham, for their technical assistance and helpful discussions to make this research work successful.

TABLE OF CONTENTS

ABSTRACT	ii
ACKNOWLEGEMENT	iii
TABLE OF CONTENTS	iv
LIST OF FIGURES	vi
LIST OF TABLES	x

Chapter		page
1.	Introduction	1
2.	Review on the properties of hydrogenated amorphous silicon	4
	2.1 Introduction	4
	2.2 Structural properties	5
	2.2.1 Compositional heterogeneity	7
	2.2.2 Structural heterogeneity	7
	2.3 Optical properties	10
	2.3.1 Optical properties well above the absorption edge	10
	2.3.2 Optical absorption edge	11
	2.4 Electrical properties	13
	2.4.1 Dark conduction	15
	2.4.2 Photoconduction	16
	References	17
3.	Microwave plasma system and characterization techniques	18

Chapter			page
	3.1	Introduction	18
	3.2	Kinetics of plasma deposition of a-Si:H films	19
	3.3	Microwave plasma systems	25
	3.4	Characterization techniques	29
		3.4.1 Structural properties	29
		3.4.2 Optical properties	33
		3.4.3 Electrical properties	35
		References	37
4.	Effects of substrate bias on the properties of a-Si:H films fabricated by ECR microwave plasma CVD		39
	4.1	Introduction	39
	4.2	Experimental details	40
	4.3	Results and discussion	44
		4.3.1 Film thickness and x-ray diffraction	44
		4.3.2 Plasma parameters	44
		4.3.3 Deposition rate and morphology	47
		4.3.4 Optical properties	54
		4.3.5 Electrical properties	66
	4.4	Conclusions	73
		References	74
5.	Conclusions		77

LIST OF FIGURES

Figure		page
2.1	Density of states models: (a) an ideal crystalline semiconductor, (b) the CFO model shows the overlapping conduction and valence band tails, (c) the Davis-Mott model shows the non-overlapping band tails but with a band defect level near midgap. Localized states are shown shaded.	6
2.2	NMR line shapes of a-Si:H film (left hand side) and the same film after annealing at 400°C (right hand side). Top curves are experimental data, and bottom curves show deconvolution of data into broad and narrow components.	8
2.3	Spectrum of the imaginary part of the dielectric constant, ε_2, for (1) crystalline Si, (2) glow discharge a-Si:H, (3) CVD a-Si, and (4) evaporated a-Si.	12
2.4	Absorption edge spectrum of glow discharge a-Si:H, determined from direct measurements of optical transmission, from collection efficiency and from photoconductivity.	14
3.1	Schematic diagram showing the intermediates and products produced by the further reaction of the primary fragments, according to the reactions listed in Table 3.1. The primary fragments are shown in squares.	24

Figure		page

3.2 Overall system configuration. 27

3.3 Schematic diagram showing the ECR microwave system chamber. 30

4.1 Top view of waveguide chamber showing the positions of table and floor substrates. 41

4.2 Typical x-ray diffraction pattern (Cu-Kα) as a function of scattering angle for a-Si:H films. 45

4.3 Probe I-V characteristic measured by Langmuir plane probe in a H_2 plasma at 1 mTorr with 4 W absorbed microwave power. V_f, the floating potential, and V_p, the plasma potential are also indicated. 46

4.4 The quantities V_p- V_b and V_p-V_f as a function of table bias potential, V_b, as measured by Langmuir probe in a H_2 plasma at 1 mTorr with 4 W absorbed microwave power. 48

4.5 Deposition rate of a-Si:H films deposited on the floor and the table as a function of table bias. 49

4.6 Scanning electron micrograph of the fracture surface of a-Si:H (floor sample) deposited at a table bias V_b=0, illustrating the columnar structure. 53

Figure page

4.7 IR absorption spectrum of a table sample with table bias, V_b = -100 V. Absorption bands for monohydride are stretching and wagging modes 55

4.8 The refractive index, n, as a function of photon energy for a-Si:H films deposited on glass substrates, i.e., floor samples, for various table bias, V_b. 56

4.9 The refractive index, n, as a function of photon energy for a-Si:H films deposited on stainless steel substrates, i.e., table samples, for various table bias, V_b. 57

4.10 The imaginary part of the dielectric constant, ε_2, as a function of photon energy for a-Si:H films deposited on glass substrates (floor samples). 59

4.11 The imaginary part of the dielectric constant, ε_2, as a function of photon energy for a-Si:H films deposited on stainless steel substrates (table samples). 60

4.12 The maximum value of the imaginary part of the dielectric constant, ε_{2max}, as a function of table bias, V_b, for a-Si:H films deposited on glass, quartz, and stainless steel substrates. 61

4.13 Optical absorption coefficient as a function of photon energy for a-Si:H films deposited on glass substrates (floor samples) for various table bias, V_b. 64

Figure page

4.14 Optical gap E_{opt} as a function of table bias, V_b, for a-Si:H films deposited on stainless steel substrates (table samples) and glass substrates (floor samples). 65

4.15 The B-parameter of the Tauc's plot as a function of table bias, V_b, for a-Si:H films deposited on stainless steel substrates (table samples) and glass substrates (floor samples). 67

4.16 Dark conductivity and photoconductivity at room temperature as functions of table bias for a-Si:H films deposited on glass substrates (floor samples). 68

4.17 Dark conductivity and the ratio of photo- to dark conductivity as functions of table bias for a-Si:H films deposited on glass substrate (floor samples). 70

4.18 Dark conductivity and the ratio of photo- to dark conductivity as functions of table bias for a-Si:H films deposited on stainless steel (solid line) and quartz (dotted line) substrates. 71

4.19 Correlation between photoconductivity and B-parameter of the Tauc's plot for a-Si:H films deposited on glass substrates (floor samples). 72

LIST OF TABLES

Table		page
3.1	Plasma Decomposition Reactions	22
3.2	Vibrational Modes of SiH_x (x=1-3)	32
4.1	Deposition Parameters	43

CHAPTER I
INTRODUCTION

In the past 15 years, amorphous semiconductors have been extensively studied, both experimentally and theoretically. Research in this field is rapidly growing and has become one of the most active areas in condensed-matter physics. This growing interest can be understood, since the unique properties of these new semiconductors, together with state-of-the-art technologies in large area thin films, open many possibilities for opto-electronic device applications. Of the amorphous semiconductors, hydrogenated amorphous silicon (a-Si:H) is certainly the most important, since it was the first amorphous semiconductor which could be doped n-type or p-type, where hydrogen seems to play an important role in making this type of doping possible. Also, hydrogenated amorphous silicon is a direct band gap material and can absorb light energy greater than ~ 1.7 eV efficiently. As a result, it thus absorbs in a film ~ 0.5 μm thick as much sunlight as does crystalline silicon (an indirect band gap material) in a 50 μm thick sample. As a consequence, this material has been widely applied to semiconductor devices, such as photovoltaics devices, particularly solar cells, photosensitive devices, thin film transistors and charge-coupled devices.

Of all the fabrication techniques, radio-frequency plasma chemical vapor deposition method has become the most promising and preferred technique to fabricate these a-Si:H films with sufficiently good characteristics for those semiconductor devices. However, this fabrication technique suffers several problems. For example, it is not easy to realize a high deposition rate and it may also suffer

contamination problems if the powered electrodes are immersed in the plasma. Further, since substrates are located in the plasma regions, it is thus considered that plasma damage due to high energy charged particles would occur.

In order to eliminate all these problems, an electron cyclotron resonance (ECR) microwave plasma chemical vapor deposition (CVD) method has been used to fabricate a-Si:H films. As this method uses microwave power and satisfies the ECR condition, the plasma is electrodeless and well-confined. This plasma can absorb power efficiently and dissociate gases effectively. It is thus considered that this microwave plasma techniques may be superior to other plasma techniques.

It is well known that the charged particles, as well as the radicals, play an important role in a-Si:H film formation. Although the contribution of the charged particles is not yet well understood, it is believed that the enhancement of ion flow by a negative bias is advantageous for the improvement of a-Si:H film characteristics.

The intent of this thesis is to investigate the bias effects on a-Si:H films fabricated by ECR microwave plasma. Through this study, it is hoped that a better understanding of the profound effects by the charged particles during film growth can be obtained.

This thesis primarily comprises (i) fundamental studies of structural, optical and electrical properties of a-Si:H films, (ii) characterization of a-Si:H thin films fabricated in ECR microwave plasma system, with emphasis on the effects of substrate bias. Chapter two reviews the fundamental properties of amorphous silicon. Chapter three presents overviews on plasma kinetics, ECR microwave plasma system, and the characterization techniques used in this thesis. Chapter four deals with the main subject of this thesis,

which is an experimental investigation on the effects of substrate bias on the a-Si:H thin films. Finally, chapter five summarizes the results of this work and presents the overall conclusions.

CHAPTER II
REVIEW ON THE PROPERTIES OF HYDROGENATED AMORPHOUS SILICON

2.1 Introduction

In this chapter, we shall review some of the basic properties of hydrogenated amorphous silicon (a-Si:H), with emphasis on the structural, optical and electronic properties.

In general, the constituent atoms of an amorphous material are not arranged in a periodic fashion, which means that the long-range order is absent. However, due to a limited number of bonding configurations available to the individual atoms, the short-range order is still present in the neighbourhood of each atom. Without periodicity, that is, lack of the long-range order, the Bloch theorem is no longer applicable and the electron state cannot be described by well-defined k (wavevector) values. Therefore, the momentum selection rule for optical transitions is relaxed, resulting in more contribution to the absorption spectra. However, allowed bands and energy gaps still occur because the density of states (DOS) is controlled most strongly by the local electron bonding configurations, that is, the short range order. Since there is an electronic DOS, the occupancy of these states must still be described by the Fermi-Dirac distribution, $f(E)$.

In an ideal crystalline semiconductor, the density of states has a form of sharp structure, where bands of extended states are separated by a forbidden energy gap as shown in Figure 2.1(a). It is considered that the density of states distribution in amorphous semiconductor should be of similar form to that of the crystalline counterpart, with some modification. Of the electrical models for

amorphous semiconductor, the Cohen-Fritzsche-Ovshinsky (CFO) model is one of the important models that is presently in use. This model, as shown in Figure 2.1(b), consists of tail states extended across the forbidden gap in a structureless distribution. These tails of localized states may overlap and pin the Fermi level near the midgap. Two critical energies for which carrier mobility increases sharply, are now defined as the band edges, and the separation as the "mobility gap" [2.1]. This model is considered to be relevant to amorphous silicon. However, the most popular electronic model for the density of states distribution is the Davis-Mott model. It was proposed on the basis of experimental results. As shown in Figure 2.1(c), localized states from conduction and valence bands extend only a few tenths of an electron-volt into the forbidden gap. The localized states near the midgap are due mainly to dangling bonds.

In the following sections, we shall confine ourselves to the discussion on hydrogenated amorphous silicon. The amorphous semiconductor draws the greatest attention of scientists and technologists at the present time.

2.2 Structural Properties

In general, a tetrahedrally bonded random network of group IV atoms relieves its large internal strain by leaving some of its atoms three-fold or five-fold coordinated, resulting in dangling bonded atoms, or floating bonded atoms, which may segregate on internal surfaces of voids. Relative to crystalline silicon, the amorphous films can have a density deficit of 15% to 40% [2.2]. The unbonded sp^3 orbitals contain only one electron and hence can be detected by electron spin resonance (ESR). In amorphous silicon (a-Si), the abundance of dangling Si bond states in the gap makes it insensitive to

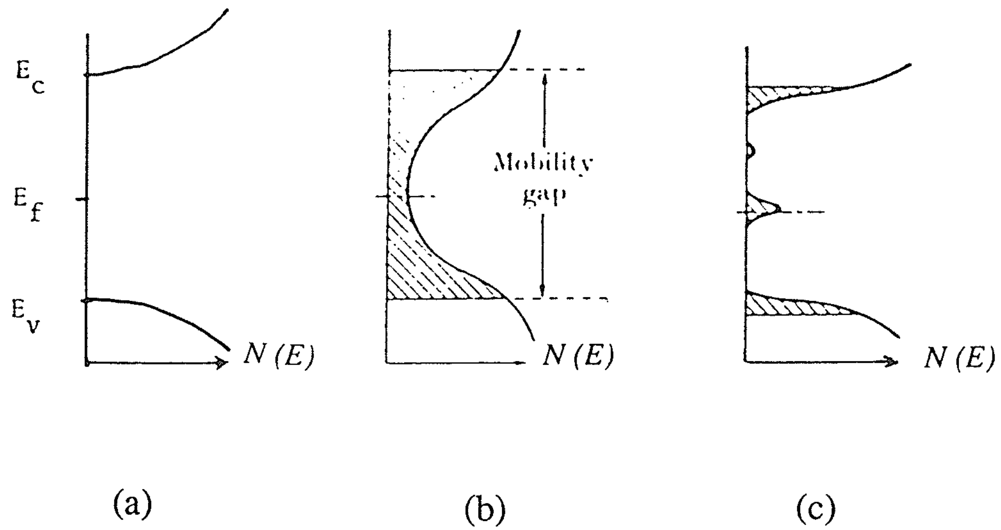

Figure 2.1 Density of states models: (a) an ideal crystalline semiconductor, (b) the CFO model shows the overlapping conduction and valence band tails, (c) the Davis-Mott model shows the non-overlapping band tails but with a band defect level near midgap. Localized states are shown shaded.

doping and "electronically messy". In hydrogenated amorphous silicon (a-Si:H) the gap is relatively free of states and is described as "electronically clean". As a consequence, this material can be doped and shows many of the desirable semiconductor properties.

2.2.1 Compositional Heterogeneity

In a-Si:H, hydrogen is considered to have removed most of the gap states because a silicon dangling bond prefers to bond to a hydrogen atom. However, there are still a number of localized states extending as tails from the conduction and valence band into the gap. These are believed to originate from dihedral angle variations and from odd-numbered silicon rings in the amorphous network [2.3]. These states would strongly affect the transport properties but not the recombination lifetime of excess charge carriers.

On the basis of proton nuclear magnetic resonance (NMR) studies [2.4,2.5], glow discharge a-Si:H films appear to contain two-phase compositional heterogeneities where (1) the hydrogen is randomly dispersed, diluted and bonded as monohydride, and (2) the hydrogen is clustered and either bonded as monohydride or polyhydride. The average separation of protons, that is, the dipole-dipole interaction, affects the width of NMR signal which allows the distinction of the two phases as a broad and a narrow-line component, as shown in Figure 2.2. In general, all glow-discharge a-Si:H films prepared under different conditions have been reported to exhibit these two components.

2.2.2 Structural Heterogeneity

It has been thought that the growth conditions of glow discharge decomposition, together with the presence of hydrogen,

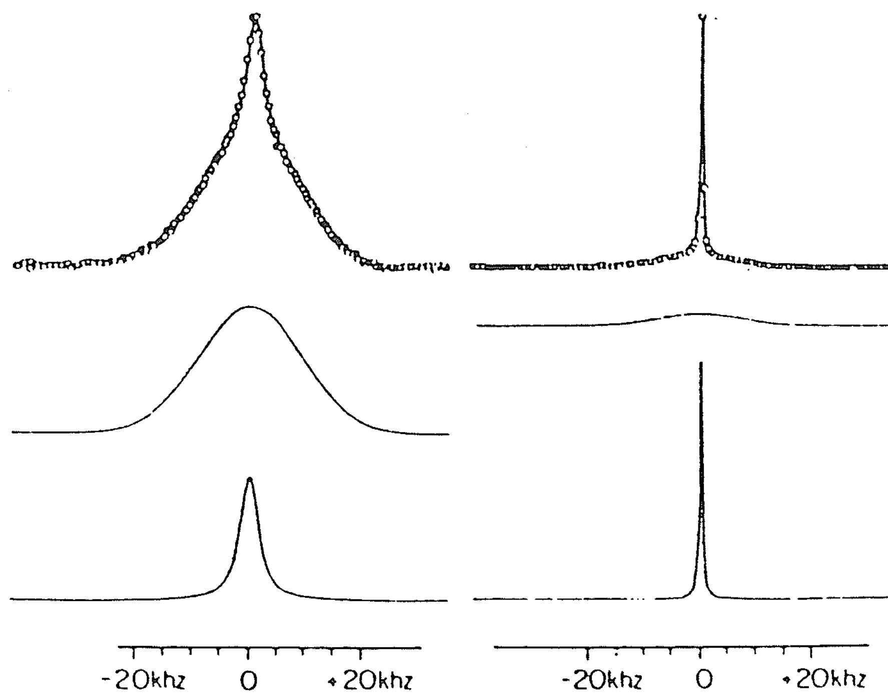

Figure 2.2 NMR line shapes of a-Si:H film (left hand side) and the same film after annealing at 400°C (right hand side). Top curves are experimental data, and bottom curves show deconvolution of data into broad and narrow components.(After ref. 2.4)

provide a continuous network which is free of structural inhomogeneity and yield the device qualities of the a-Si:H film. However, Knights et al. [2.6,2.7] have discovered a columnar growth morphology in a-Si:H film grown under a variety of glow discharge conditions. The columns of 100-300 Å lateral dimensions grow vertically from the substrate. Further, columnar growth becomes more pronounced when SiH_4 is diluted with inert gases of larger molecular weight. Films having gross structural inhomogeneity usually exhibit low luminescence and poor photoconductivity. On the other hand, films having device quality show no discernible microstructure. However, it has been suggested [2.6,2.7] that the apparent homogeneity can be attributed to the reduction of the visible definition of the interstitial regions. The deposition conditions would not change the growth pattern significantly. Instead, they affect the coalescence of the columns and the amount of the second phase in the intercolumnar space.

Since NMR studies reveal that all films contain two phases having different hydrogen concentrations. The high hydrogen content phase contains all the polyhydride species and some monohydride whilst the dilute phase contains only monohydride. Reimer et al. [2.8] have suggested that the dilute phase represents the bulk regions of the grains making up the film, whereas the highly dense phase fills the intergrain spaces.

Films having pronounced columnar growth structure are usually 20-40 % less dense than crystalline Si and are naturally quite porous. Therefore, they are unstable upon exposure to atmosphere, leading to post-deposition contamination effects.

2.3 Optical Properties

The optical properties of amorphous silicon are determined by its electronic band structure. Since the dielectric function depends sensitively on the electronic band structure of the material, therefore studies of the dielectric function, particularly the imaginary part, ε_2, are very useful in determining the optical properties of a material.

2.3.1 Optical Properties Well Above the Absorption Edge

Assuming parabolic bands, the optical gap E_{opt} is defined by [2.9]

$$\alpha h\nu = B(h\nu - E_{opt})^2 \qquad (1)$$

where α is the absorption coefficient and $h\nu$ is the photon energy. In an amorphous material, since k is no longer a good quantum number due to lack of long range order, all pairs of states (between filled at energy E, and empty at energy $E + h\nu$) can be assumed to participate in optical transitions [2.10]. By assuming constant matrix elements over a small range of energies near the absorption edge, the imaginary part of the dielectric constant can be written

$$\varepsilon_2 (h\nu) = const. \int n_v(E)\, n_c (E + h\nu)\, dE \qquad (2)$$

where $n_v(E)$ and $n_c(E)$ are the density of states of the valence and conduction bands, respectively. Assuming parabolic bands at the band edges, $n_v(E) \propto (E_v - E)^{1/2}$ and $n_c \propto (E - E_c)^{1/2}$ as in crystalline material, ε_2 becomes $\varepsilon_2 \propto (h\nu - E_{opt})^2$ where $E_{opt} = E_c - E_v$, and E_c and E_v are the conduction and valence band edges, respectively. Therefore, the absorption coefficient $\alpha (h\nu)$ is also given by

$$\alpha(h\nu) = 2\pi\varepsilon_2(h\nu) / n\lambda \qquad (3)$$

where n is the refractive index, and λ is the wavelength. Figure 2.3 shows the imaginary part of the dielectric constant for different amorphous Si films and crystalline silicon. The sharp features in the spectrum for crystalline silicon, which are related to the band structure, are missing for all the amorphous silicons. Nevertheless, the overall width and shape of the spectrum are about the same. Also, the spectra of different amorphous films depend critically on preparation conditions. The ε_2 peak of the glow discharge a-Si:H occurs at a higher energy and reaches a much larger value than the a-Si films without hydrogen content. These results suggest that the bonding in the amorphous network has been considerably altered by hydrogen. The shift of ε_2(max) to a lower photon energy in both evaporated and CVD materials suggests a greater incidence of weak bonds, that is, the silicon tetrahedra are distorted [2.11]. However, it is not possible to come to a conclusion about altered transition matrix elements from the variable peak heights without more knowledge about the relative mass densities of the films.

2.3.2 Optical Absorption Edge

In general, the optical absorption curve $\alpha(h\nu)$ of amorphous semiconductors consists of three parts [2.9]:

(1) At high energies, and $\alpha > 10^4$ cm^{-1}, where the absorption coefficient is described by Eqn. (1). Here, B contains an average matrix element, constant with energy, and the joint density of states for the conduction and valence bands. Since the crystal momentum selection rule is broken by the disorder, therefore the value of B is much greater than that in the crystal. It is this fact that makes these

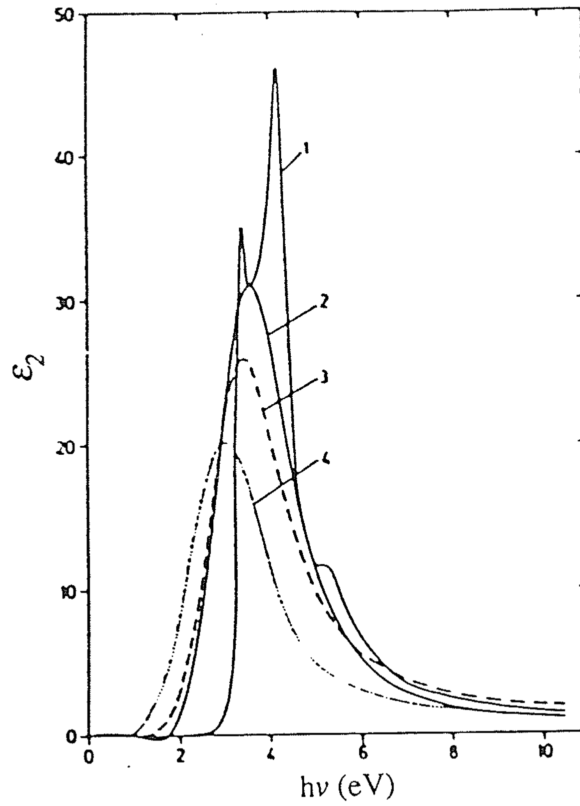

Figure 2.3 Spectrum of the imaginary part of the dielectric constant, ε_2, for (1) crystalline Si, (2) glow discharge a-Si:H, (3) CVD a-Si, and (4) evaporated a-Si. (After ref. 2.11)

materials viable candidates for thin film solar cells.

(2) At intermediate energies, ($10^2 < \alpha < 10^4$ cm^{-1}), by an exponential variation of α with $h\nu$.

$$\alpha(h\nu) = \alpha_0 \exp(h\nu / E_1) \quad (4)$$

With a slope parameter E_1 which is typically between 0.05 and 0.08 eV. This has been variously attributed to exponential tails of states to the valence and conduction bands, or to photon-assisted tunneling in the presence of potential fluctuation.

(3) At the lowest photon energies and absorption coefficients, by an absorption which is quite variable and is commonly related to defect and impurity states. Figure 2.4 shows a typical edge for glow discharge a-Si:H film. The energy gap E_{opt} is defined as the intercept of the $(\alpha h\nu)^{1/2}$ vs. $h\nu$ curve in region (1). Further, the "intrinsic" part of an edge occurs for $\alpha > 10^4$, and $\alpha \approx 10^4$ makes the demarcation line between "intrinsic" edge and a defect dominated edge. The optical gap E_{opt} of glow discharge a-Si:H films fall between 1.6 and 1.85 eV which is considerably higher than that of sputtered or evaporated films [2.12,2.13]. This is mainly due to the substantial hydrogen content in a-Si:H films, since Si-H bonds are stronger than Si-Si bonds.

2.4 Electrical Properties

In this section, we review the dark and photo-conductivity phenomena of hydrogenated amorphous silicon based on the Davis-Mott [2.1] model of amorphous semiconductors.

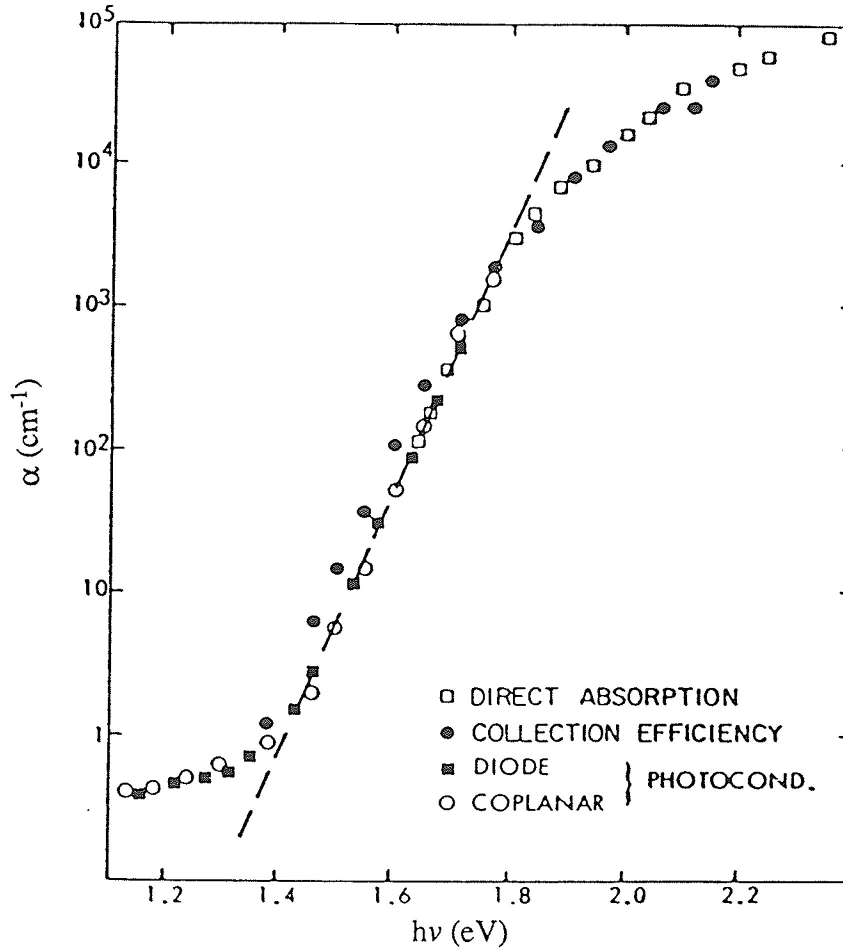

Figure 2.4 Absorption edge spectrum of glow discharge a-Si:H, determined from direct measurements of optical transmission, from collection efficiency and from photoconductivity. (After ref. 2.12, 2.13)

2.4.1 Dark Conduction

Based on the Davis-Mott model, we describe the dark conductivity by

$$\sigma_d = \sigma_1 exp(-E_1/ kT) + \sigma_2 exp(-E_2/ kT) + \sigma_3 exp(-C_3/ T^{1/4}) \quad (5)$$

The first term on the right side of the equation is the extended state conduction which occurs for electrons above the conduction band edge or holes below the valence band edge in a manner that analogous to that in crystalline materials. At high temperature, extended state conduction is dominant and the typical values of the pre-factor, σ_1, lies between 10^3 and 10^4 mho/cm while the activation energy, E_1, lies between 0.65 - 0.95 eV.

The second term of the equation refers to hopping conduction in the band tails where σ_2 is equal to $q\mu N_c$, where N_c is the effective density of states in the conduction band and μ is the hopping mobility. E_2 can also be written as $E_2 = -(E_A - E_F + w_1)$ where w_1 is the hopping activation energy and E_A is an arbitrary energy within the range of tail states. However, this kind of band tail conduction will not be dominant if the density of defect states at the Fermi level is high and, therefore, is rarely observed.

The third contribution of dark conductivity in amorphous semiconductors is the variable range hopping in a band of defect states at the Fermi-level. C_3 is equal to $[18\ \lambda^3/\ kN(E_f)]^{1/4}$ where λ is the decay rate of the localized wave functions, and $N(E_f)$ is the density of localized states at the Fermi-level. σ_3 contains a $T^{-1/2}$ dependence, therefore at low temperature where variable range hopping

conduction is dominant, a plot of $ln(\sigma_d T^{1/2})$ vs. $1/T^{1/4}$ will be linear.

2.4.2 Photoconduction

Photoconductivity is defined as the excess conductivity produced by optical excitation. If we only consider the dominant electron flow, the photoconductivity of a hydrogenated amorphous silicon film is given by [2.14].

$$\sigma_{ph} = qG\mu\tau, \tag{6}$$

where τ is the recombination lifetime, μ is the electron mobility, q is electron charge and

$$G = \eta F(1 - R)[1 - exp(-\alpha d)] / d \tag{7}$$

is the electron-hole generation rate. $F(1 - R)$ is the incident photon flux correct for surface reflection, η is the quantum efficiency, α is absorption coefficient, and d is the semiconductor thickness.

Typical values of photoconductivity for a-Si:H films are between 10^{-7} - 10^{-3} mho/cm. Compared to those of dark conductivity which are between 10^{-11} - 10^{-7} mho/cm, the high σ_{ph}/σ_d ratio is very useful for photosensitive device applications.

References

[2.1] N.F. Mott and E.A. Davis, "Electronic Processes in Non-Crystalline Materials", (Clarendon, Oxford, 1979).

[2.2] E.C. Freeman and W. Paul, Phys. Rev. B, **20** (1979) 716.

[2.3] H. Fritzsche, J. Non-Cryst. Solids **76** (1985) 157.

[2.4] J.A. Reimer, R.W. Vaughan, and J.C. Knights, Phys. Rev. B, **24** (1981) 3360.

[2.5] S. Hayashi, K. Hayamizu, S. Yamasaki, A. Matsuda, and K. Tanaka, J. Appl. Phys. **56** (1984) 2658.

[2.6] J.C. Knights and R.A. Lujan, Appl. Phys. Lett. **35** (1979) 244.

[2.7] J.C. Knights, J. Non-Cryst. Solids **35** & **36** (1980) 159.

[2.8] J.A. Reimer, R.W. Vaughan, and J.C. Knights, Phys. Rev. Lett. **44** (1980) 193.

[2.9] J. Tauc, "Amorphous and Liquid Semiconductors", (Plenum, New York, 1974) p.159.

[2.10] R. Zallen, "The Physics of Amorphous Solids", (Wiley, New York, 1983) p.266.

[2.11] D. Ewald, M. Milleville, and G. Weiser, Philos. Mag. B **40** (1979) 291.

[2.12] R.J. Loveland, W.E. Spear and A. Al-Sharbaty, J. Non-Cryst. Solids **13** (1973) 55.

[2.13] J.I. Pankive, F.H.Pollak and C. Schnabolk, J. Non-Cryst. Solids **35** & **36** (1980) 459.

[2.14] W. Beyer and B. Hoheisel, Solid State Commun. **47** (1983) 573.

CHAPTER III
MICROWAVE PLASMA SYSTEM AND CHARACTERIZATION TECHNIQUES

3.1 Introduction

In this chapter, we shall present a brief outline of the fabrication techniques for preparing hydrogenated amorphous silicon and the plasma growth kinetics. We shall then briefly describe the novel microwave plasma system developed in our Materials and Devices Research Laboratory at the University of Manitoba, where the a-Si:H thin films under investigation being presented in this thesis were fabricated. Finally, the details of the main characterization techniques used in this thesis are given.

There are many techniques to prepare a-Si:H thin films which by far is the most common available form. These techniques include evaporation, reactive sputtering, chemical vapor deposition (CVD), and the most widely used glow discharge techniques.

Evaporation of silicon without hydrogen can produce high purity amorphous silicon films, but in this case subsequent hydrogenation by exposuring the films to atomic hydrogen is needed [3.1]. Reactive sputtering is a well-developed industrial process capable of fast deposition [3.2]. In this technique, a solid silicon target is bombarded by ions, usually argon, and sputtered Si atoms are then condensed onto the substrate. A controlled amount of hydrogen added to the sputtering gas is atomized and reacts with the sputtered Si, thus facilitating the incorporation of atomic hydrogen to the silicon films. In chemical vapor decomposition, silane is decomposed at 450°C and the amorphous films are then deposited. This technique suffers from

small hydrogen content and low deposition rate. When disilane instead of silane is employed, the deposition rate is much enhanced and can proceed at much lower temperatures, therefore reducing the amount of hydrogen evolved [3.3]. To enhance incorporation of hydrogen, homogeneous CVD (HomoCVD) has been developed, where the substrate is cooled by nitrogen. This technique produces amorphous silicon films containing a high concentration of hydrogen and a low concentration of dangling bonds [3.4]. Probably the most popular technique for fabricating a-Si:H is the glow discharge of silane, also referred to as the plasma enhanced chemical vapor decomposition (PECVD). In this process an electric field (dc, ac, rf, microwave) is used to produce a plasma which contains ions and reactive species. In this technique the radicals condense on a heated substrate (typically about 100-400°C) to form an amorphous silicon film. Hydrogenated amorphous silicon deposited by this technique is found to have good structural, chemical and electronic properties but they are very dependent on the deposition conditions.

3.2 Kinetics of Plasma Deposition of a-Si:H Films

Hydrogenated amorphous silicon (a-Si:H) prepared by rf and dc glow discharge of silane has been extensively studied for the purpose of its widely applications. However, the growth kinetics or the deposition mechanisms are still not well understood and remain as open questions. Mass spectrometry and optical emission spectrometry studies are now beginning to give some answer to these questions. In this section, we describe briefly the rf and dc glow discharge of silane deposition processes. Since microwave plasma techniques are still in research stage, therefore, it is hoped that through comparative studies

of rf and dc glow discharge depositions, we may get some insight into the ECR microwave plasma deposition processes.

Plasma deposition primarily consists of three main processes, which are, (i) plasma excitation and decomposition which produce the reaction species, (ii) gas reaction of these species while diffusing or drifting to the substrate, (iii) surface reactions including compiling and reemission at the substrate surface. It is beyond the scope of this thesis to discuss in detail a growth model of a-Si:H, we shall confine ourselves to describe only the first two main processes of the plasma deposition processes.

In general, a glow discharge is initiated and maintained by inelastic collisions between electrons and molecules. As the molecules are excited, they become unstable and may be decomposed, ionized or both. The rates of these reactions are given by [3.5]

$$r_i = n_e k_i [X] \qquad (1)$$

where n_e is the electron concentration, k_i is the rate constant for the reaction, and $[X]$ is the concentration of X. The rate constant is given by

$$k_i = (2 / m_e)^{1/2} \int E^{1/2} f(E) \sigma_i(E) dE \qquad (2)$$

where m_e is the electron mass, $f(E)$ is the normalized electron energy distribution and $\sigma_i(E)$ is the cross section for the reaction which is a function of energy. Although the electron energy distribution may not be Maxwellian, it is always assumed to be so for simplicity.

The primary decomposition reactions are the most important reactions for the properties of the deposited films, since they are known to produce both ions and neutral radicals which are responsible

for the film growth. Since enthalpies of all the ions and neutral radicals are known, it is possible to calculate the energy required to produce them [3.6]. Table 3.1 lists all the major reactions including electron-impact dissociations and ionizations. Another important reaction should also be considered, that is the dissociation of H_2, which is a product of the deposition process and is always used as diluent of silane;

$$H_2 + e^- \text{ --------> } 2H + e^- \qquad (\approx 99 \text{ Kcal/mol}) \qquad (3)$$

Further, reactions similar to (b), (d), (e) and (g)[see Table 3.1], in which 2H is produced instead of H_2, would require 99 Kcal/mol or more energy for each H_2 dissociated. From the table it is clear that the species formed by electron impact decomposition of silane are SiH_n (n=0-3), H, H_2 and SiH_n^+ (n=2,3). Other positive ions, Si^+, SiH^+ and SiH_4^+ ion are either scarce or unstable, therefore they are not observed in mass spectrometric studies. The mean electron temperature, T_e, of silane plasma has been measured to be 0.5 - 5.0 eV (11.5 - 115 Kcal/mol) [3.7]. Thus, ionization process, such as (a) and (b) in Table 3.1 would arise from the high energy tail of the electron distribution. It has been observed that SiH_2^+ and SiH_3^+ are the most abundant ions in low pressure dc discharge (< 5 mTorr) [3.8,3.9]. On the other hand, the relatively large number of low energy electrons in the distribution may prove that reactions (f) and (g) are the most important processes which result in large quantities of SiH_2 and SiH_3 [3.9]. All these species arising from the primary processes are very

TABLE **3.1**

PLASMA DECOMPOSITION REACTIONS (After ref. 3.6)

Reaction	ΔH (kcal mol^{-1})
1. Primary Processes	
a. $e^- + SiH_4 \rightarrow SiH_3^+ + H + 2e^-$	284
b. $\rightarrow SiH_2^+ + H_2 + 2e^-$	263
c. $\rightarrow SiH_2 + 2H + e^-$	155
d. $\rightarrow SiH + H_2 + H + e$	131
e. $\rightarrow Si + 2H_2 + e^-$	97
f. $\rightarrow SiH_3 + H + e^-$	90
g. $\rightarrow SiH_2 + H_2 + e^-$	56
2. Secondary reactions	
1. $SiH_3^+ + SiH_4 + M \rightarrow Si_2H_7^+ + M$	—
2. $SiH_3^+ + SiH_4 \rightarrow Si_2H_5^+ + H_2$	−2.9
3. $SiH_2^+ + SiH_4 \rightarrow SiH_3^+ + SiH_3$	−1
4. $SiH_2 + SiH_4 \rightarrow Si_2H_6$	−49
5. $SiH_3 + SiH_3 \rightarrow Si_2H_6$	−74
6. $H + SiH_4 \rightarrow SiH_3H_2$	−17
7. $SiH_3 + SiH_3 \rightarrow SiH_2 + SiH_4$	−36
8. $SiH_3 + SiH_3 \rightarrow SiH_3SiH + H_2$	—
9. $SiH_2 + SiH_4 \rightarrow SiH_3SiH + H_2$	—
10. $SiH_3SiH: \rightarrow \cdot SiH_2SiH_2SiH_3 \cdot$	+11
11. $SiH_3SiH + SiH_4 \rightarrow Si_3H_8$	−62
12. $SiH + SiH_4 \rightarrow SiH_3SiH_2$	−45
13. $Si + SiH_4 \rightarrow SiH_3SiH$	−34

reactive and will undergo further reactions before reaching the substrate.

Part 2 of Table 3.1 lists all the secondary reactions which are the most likely reactions of the primary fragments. Reactions (1) to (3), show the fates of SiH_2^+ and SiH_3^+ ions generated in the discharge. It has been suggested that SiH_3^+ is the precursor of the large ionic clusters, $Si_mH_n^+$ (m=2-5), as commonly observed in the plasma [3.10]. The dominant loss process of SiH_3^+ is mainly upon wall (substrate) recombination to the SiH_3 radical [3.11]. It is worth noting that reaction (3) shows SiH_2^+ to be a source of both SiH_3^+ and SiH_3. This explains why SiH_3^+ is dominant in the plasma even though SiH_2^+ is the main product of the ionization of silane [3.7,3.8]. Reactions (4) through (9) show the gas-phase reactions of SiH_2 and SiH_3 , which lead to the formation of disilane and the silylene (SiH_3SiH) fragments. Silylene radicals are important in their ability to introduce polysilane segments, $(SiH_2)_n$, into the growing film and therefore have been hypothesized as the major deposition species on the basis of SiH_4 and Si_2H_6 plasma growth [3.12]. The rest of the reactions are based on energetic consideration alone, and there is little known about these reactions.

Figure 3.1 summarizes the various fates of all the primary reactive species and their corresponding reactions. At this time, the growth mechanism of a-Si:H films is still regarded as an open question. Based on an evaporation deposition model, Knights [3.13]

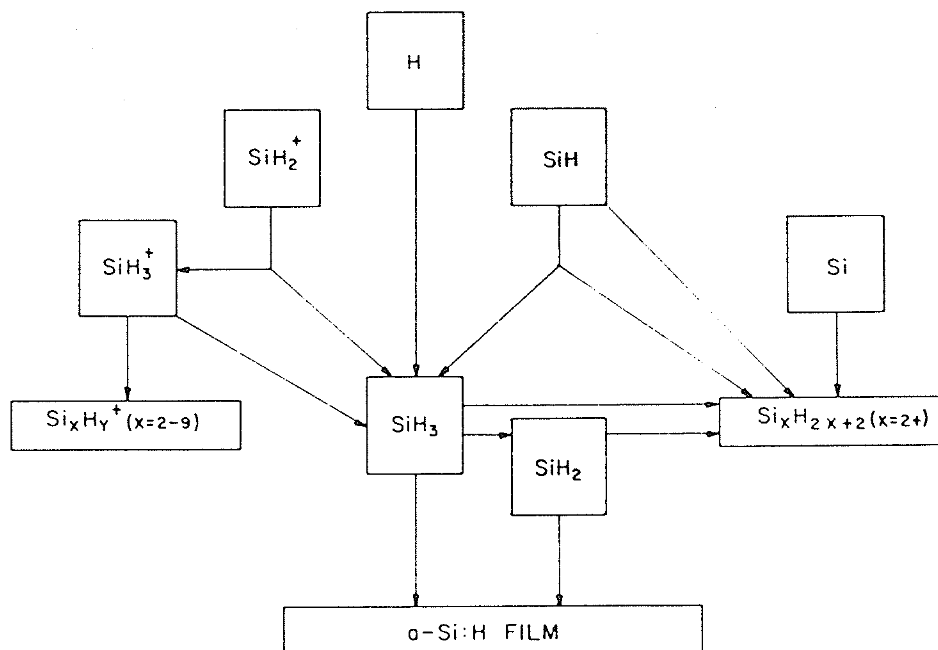

Figure 3.1 Schematic diagram showing the intermediates and products produced by the further reaction of the primary fragments, according to the reactions listed in Table 3.1. The primary fragments are shown in squares. (After ref. 3.6)

has proposed that the growth of a-Si:H films may be due to SiH_3 and SiH_2. It was then thought that SiH_2 may be a precursor to the formation of a-Si:H films with a subsequent hydrogen elimination and cross-linking [3.14]. However, Longeway [3.15, 3.16] has proposed that SiH_3, in fact, is the a-Si:H film precursor in silane discharge. He has demonstrated on the ground that the introduction of nitric oxide, NO, which is a known SiH_3 scavenger to the discharge, has led to a total suppression of the formation of a-Si:H films. He has therefore suggested that SiH_3 is an important intermediate that binds to dangling bonds at the surface of the film before losing its hydrogen. Further, recent experiments by Gallagher [3.17] also show that SiH_3 dominates neutral radical deposition by producing at least 98% of the Si deposit for typical deposition conditions (> 100 mTorr at 240°C).

The initial processes of plasma deposition and the a-Si:H film precursors are understood to some degree of certainty, though the surface reactions are still unclear. These surface reactions mainly consist of the reaction of various species, which probably depends on their stricking coefficients or reaction probabilities with the surface, also on the dehydrogenation and crosslinking steps.

3.3 Microwave Plasma Systems

The development of the microwave plasma system was originated by Mejia et al. [3.18-3.20] for the fabrication of a-Si:H thin films. The underlying motivations were to explore alternate deposition systems and to exploit their inherent advantages. Initially, the first system was a coaxial line-type system with plasma acting as a center

conductor [3.21]. This system suffered several inherent limitations, which included sputtering of the quartz discharge tube, high sustaining microwave power, incorporation of oxygen into the growing film, and radiation into the surrounding environment. A second system was then developed which primarily consisted of a copper WR-284 waveguide chamber, wherein the microwave plasma was confined by an external magnetic field. The waveguide was short-circuited by a copper mesh in order to prevent any microwave power from radiating to the surroundings. Microwave power needed to sustain the plasma was dramatically reduced to about 10 W. Films fabricated in this system were comparable to rf glow discharge films, with the exception that they suffered some copper contamination. However, this system configuration had proved itself to be a promising and viable system.

In order to avoid any of the copper contamination, a new system was constructed in stainless steel with configuration similar to the copper system. This new system has been used for fabricating amorphous thin films and for the magnetic field confinement reactive ion etching. Figure 3.2 shows the overall system configuration. This system primarily consists of a short-circuited stainless steel rectangular waveguide chamber of dimensions equivalent to a WR-284 waveguide, which is 45 cm in length. Microwave at 2.45 GHz is generated by a magnetron operating in a continuous mode and propagates to the chamber through a rectangular waveguide in the TE_{10} mode. Two external water-cooled magnetic field coils, capable of providing magnetic fields up to 1 KGauss, are arranged axially to the chamber. In this configuration, the plasma can be confined and controlled in order to prevent its contact with the walls of the waveguide chamber, thus reducing any impurity incorporation of the

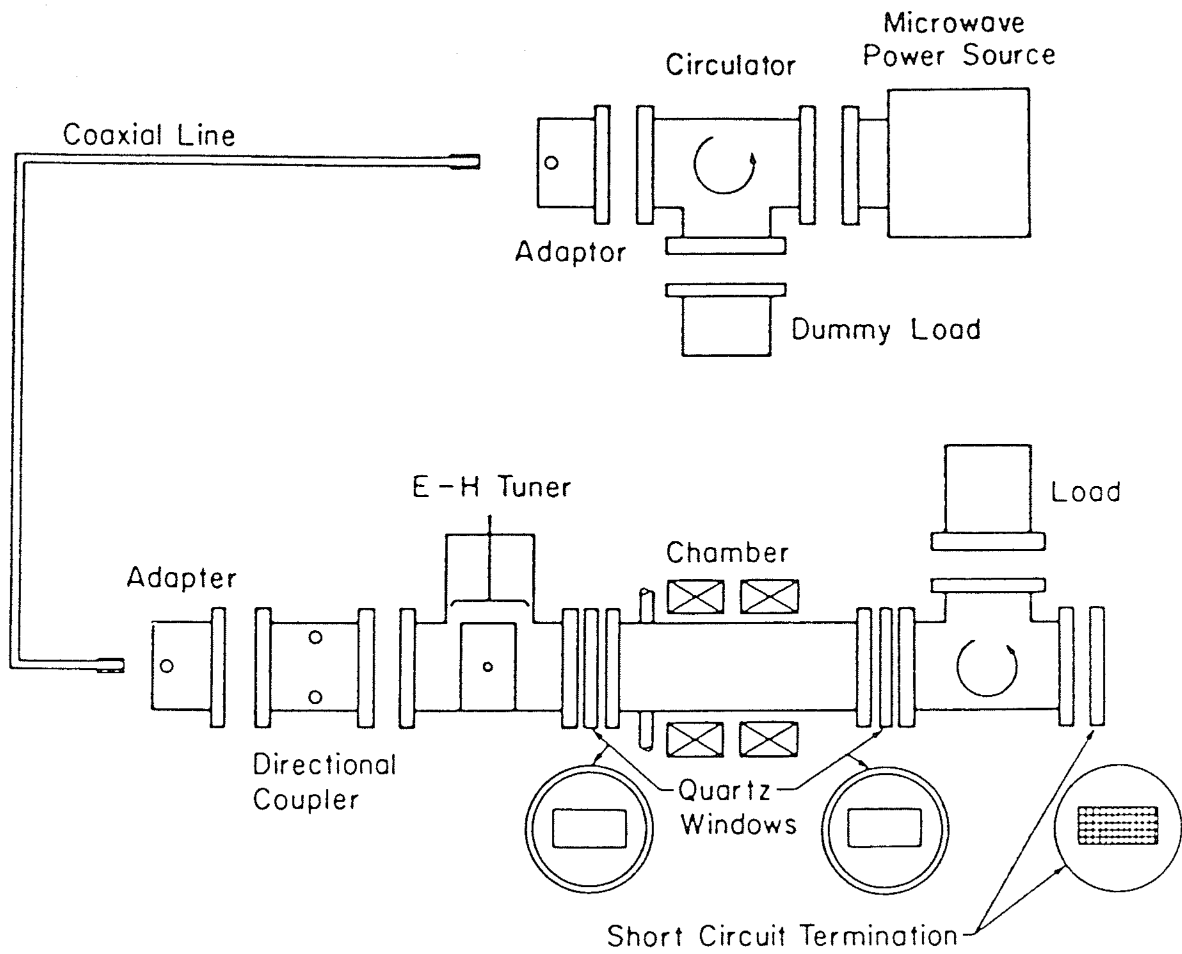

Figure 3.2 Overall system configuration.

growing films. Futher, conditions of electron cyclotron resonance (ECR) can be achieved when the magnetic field strength reaches to 875 Gauss. This can be easily accomplished by increasing the coil current to ≈ 22.5 A. ECR is a resonant condition at which the natural oscillation of an electron moving in a magnetic field corresponds to the electric field oscillation of the microwave excitation. As a consequence, plasmas under ECR conditions are found to be more stable and uniform; the system can be operated at microwave absorbed power as low as 1 W.

The vacuum system consists of an oil diffusion pump for evacuation of the chamber to a base pressure better than 10^{-6} Torr, a cold trap and a rotary pump for evacuation of gas mixture during deposition. The deposition pressure depends upon the flow rate of the gases introduced into the chamber. The typical pressure of operation ranges from 10^{-1} to 10^{-4} Torr. The chamber and all gas lines can be baked to 200°C. This processing system is also equipped with a Langmuir probe, an optical emission spectrometer (OES) and a mass spectrometer in order to optimize the processing conditions, since the compositions of excited molecules and the interactions among reactive species in the plasma are of fundamental importance during a-Si:H thin film deposition to the film properties.

The system has undergone cycles of modifications and improvements for studies of plasma, amorphous and dielectic thin film deposition. Currently, a single coil is employed to give a better confinement and controllability of the plasma. A thermostatically controlled table has been installed above the diffusion pump port, which allows substrate surfaces to be held perpendicular to the dc magnetic field lines, so that the effects of charged particles impinging

on the growing film can be studied. A modified waveguide chamber is shown in Figure 3.3.

3.4 Characterization Techniques

In this section, we describe briefly the main characterization techniques used in this investigation. These techniques have been employed [3.18-3.22] for measuring and analyzing the structural, optical and electrical properties of a-Si:H and μc-Si:H thin films.

3.4.1 Structural Properties

Structure and morphology are probably the most fundamental properties of thin films characterization. The motivations for performing these measurements in our studies are basically to determine whether or not the films are amorphous and to examine their structure and composition.

Diffraction of X-rays by a crystal can be regarded as a scattering phenomenon by successive planes of atoms within the crystal. The scattered X-rays will reinforce in certain directions and cancel in others. The directions of the reinforcement are given by Bragg's law, i.e., $n\lambda = 2d\sin\theta$, where n is the order of the corresponding reflection, λ is the X-ray wavelength, d is the spacing between the crystal planes, and θ is the scattering angle. In amorphous materials, the atoms are not arranged in a periodic fashion due to the absence of lattic periodicity and thus the rays arising from the scattering by these atoms will have a random phase relationship to one another. Therefore, the Bragg's law cannot be satisfied, which implies that sharp peaks will not be observed in an X-ray diffraction pattern. However, as a result of short range order or some degree of

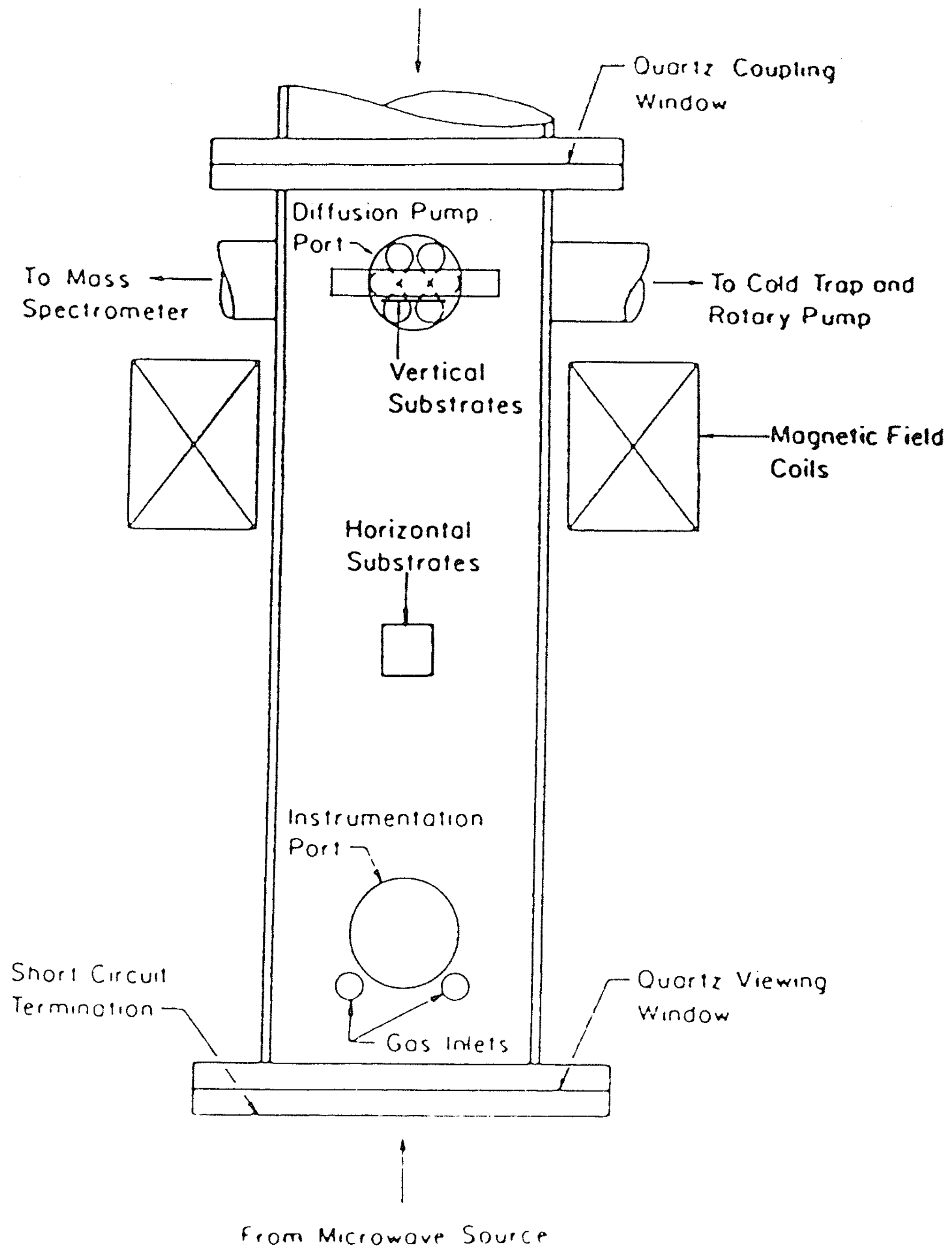

Figure 3.3 Schematic diagram showing the ECR microwave system chamber.

microcrystallinity inside the film, broad peaks are usually observed. Using X-ray diffraction method for structure determination is simple and straightforward, it has been employed to study the structure of the evaporated a-Si as well as glow discharge a-Si:H. Information on crystallite grain size, micro-strain, and volume fraction of the material can be directly obtained through the studies of diffraction line shapes [3.22, 3.23].

In our X-ray diffraction analysis, we employed a Phillips X-ray diffractometer with Cu-Kα (40 keV, 20 mA) radiation. The incident beam had a divergent slit of one degree and was attenuated by a nickel filter to prevent Compton scattering of the white X-radiation by suppressing wavelengths less than that of Cu-Kα.

In order to examine the morphology of a film, a scanning electron microscopy (SEM) is commonly employed due to its special advantages of large depth of focus and high resolution. The magnification normally varies from about 20 to 100,000X, and samples require little or no sample preparation. In general, the SEM is capable of providing sufficient information regarding the homogeneity of the material, i.e., the growth structure. An ISI Mini-SEM was employed to study the homogeneity of the fracture surface and the cross section of the a-Si:H thin films.

The IR absorption spectra of the a-Si:H films were measured using a Nicolet FTIR spectrophotometer. For this measurement crystalline silicon wafers were used as the substrate because they are transparent in the infrared frequency range. IR absorption occurs when the frequency of the incident infrared radiation is in resonance with a vibrational mode of one of the bonding configurations. By measuring the characteristic frequency, the identity of molecular

species can be determined. Thus, the IR absorption spectrum provides a unique fingerprint of the material, from which composition and structure of the material can be obtained. In particuilar, the frequency at which an absorption band occurs determines which elements are present and how they are bonded, while the height of the peak is directly proportional to the concentration of the adsorbing species in the material. Table 3.2 lists the types of the most common vibrational modes for a-Si:H and their frequencies.

Table 3.2

Vibrational Modes of SiH_x (x=1-3)

	Wavenumber (cm^{-1})		
Group	Stretching	Bending	Rocking or Wagging
SiH	2000		630
SiH_2	2090	880	630
$(SiH_2)_n$	2090-2100	890, 845	630
SiH_3	2140	905, 860	630

In addition to the types of Si-H bonds, the total hydrogren content is significantly related to films properties. The hydrogen concentration can be estimated from the following equation :

$$[Si\text{-}H] = A \int [\, \alpha(\omega) / \omega \,]\, d\omega \qquad (1)$$

Where $\alpha(\omega)$ is the absorption coefficient of the film at the

oscillating frequency ω and A is 1.6×10^{19} cm^{-2} based on the absorption intensity for the absorption band at 640 cm^{-1} [3.24]. The concentration in terms of the atomic density is calculated on the basis of the atomic density of crystalline Si, which is 5×10^{22} cm^{-3}.

3.4.2 Optical Properties

A Cary 14 spectrophotometer was employed to measure the optical transmission spectrum of the a-Si:H films over the wavelength range from 0.5 to 2.6 µm. From the transmission spectrum we can determine the absorption coefficient, optical gap, and the product of refractive index (n) and sample thickness (d). The incident light radiation would transverse the sample several times causing interference fringes to occur in the transparent region where absorption is negligibly small, provided the sample thickness is uniform. This interference fringes would result in maxima and minima of the total transmitted light intensity. The product of n and d can then be determined on the basis of the condition for the occurrence of such extremum value of the total transmitted light intensity [3.25,3.26]. For two successive interference maxima, the wavelengths for maxima satisfy

$$(1/2)\, m\lambda_1 = 2nd \tag{2}$$

and those for minima satisfy

$$(1/2)\,(m+1)\,\lambda_2 = 2nd \tag{3}$$

where m is an even integer. However, we cannot obtain either n or d directly from these equations alone. Using the thickness measured

with the Sloan stylus instrument, one is able to estimate the refractive index and these values are further confirmed by those from ellipsometric measurements.

Ellipsometry has been demonstrated to be a powerful technique for measuring the optical constants and the thickness of the thin films [3.26, 3.27]. For the null ellipsometry, the principle used is to measure the polarization of incident polarized light before and after its reflection from the surface of the film. Two indirectly measurable ellipsometric angles, ψ and Δ which represent the amplitude ratio and phase difference between the reflectances for the two linearly polarized states, are obtained from the analyzer and the polarizer, respectively. These two angles are related to the physical property of the thin film by the relation :

$$\rho = (\gamma_p / \gamma_s) = tan\psi \; exp(i\Delta) \tag{4}$$

where ρ is the complex reflectance ratio, γ_p and γ_s are the complex reflectances for light polarized parallel *(p)* and perpendicular *(s)* to the plane of incidence respectively. The quantity, ρ, is determined by the nature of the specular interface which, in our study, is assumed to be a perfect dielectric discontinuity between two homogeneous media, namely the ambient (air) and the film itself. Then the complex refractive index n^* of the film can be solved in terms of ρ and the incident angle, ϕ_o,

$$n_1^*/n_0^* = sin\phi_o[1+(1-\rho/1+\rho)^2 \; tan^2\phi_o]^{1/2} \tag{5}$$

where n_o^* is the refractive index of air.

Since the complex refractive index n^* is defined as

$$n^* = n - jk \tag{6}$$

where n is the refractive index and k is the extinction coefficient, we can obtain the complex dielectric constant, ε^*, defined as

$$\varepsilon^* = \varepsilon_1 - j\,\varepsilon_2 \tag{7}$$

by the relation $\varepsilon^* = n^{*2}$. Thus, we immediately obtain

$$\varepsilon_1 = n^2 - k^2 \tag{8}$$

and

$$\varepsilon_2 = 2nk \tag{9}$$

Also, the absorption coefficient α can be related to the extinction coefficient k by

$$\alpha = 4\pi k / \lambda \tag{10}$$

All the optical constants were measured over the photon energy range 2.0 to 3.5 eV, using spectrally-resolved ellipsometry. The Gaertner model L119 ellipsometer used for this measurement consists of a Babinet-Soleil model L135 compensator, a Bausch-Lomb grating monochromater, a Xenon light source, and a mica quarter-wave plate. Measurement error is within 5%.

3.4.3 Electrical Properties

General information about the electrical properties can be obtained through the measurement of the dark conductivity and the photoconductivity. The interpretations of the results are not unambiquous. In this study, temperature dependence of the dark and the photo-conductivities have been measured for all the a-Si:H films in the temperature range of 295°K to 380°K. The measurements were carried out in a cryogenic vacuum unit at a pressure of about

0.1 Torr. Coplanar gap cells with aluminum electrodes formed by vacuum evaporation through a metal mask were employed. For these measurements, a dc voltage of 100 V was applied between the electrodes and the electric field was ≈ 700 Vcm^{-1}, which was in the ohmic region for all films. The current was measured by a Keithley 610C electrometer operating in the fast mode. The photoconductivity was measured at a wavelength of 6328 Å with a photon flux of 10^{15} $photon.s^{-1}.cm^{-2}$. Activation energies for all films were determined from a plot of conductivity against 1000/T. Experimental error is less than 5%. The quality or the merit of the films is usually determined by the photoconductive ratio, that is, the ratio of the photoconductivity to the dark conductivity.

References

[3.1] N. Sol, D. Kaplan, D. Dieumegard, and D. Dubrevil, J, Non-Cryst. Solids **35** (1980) 291.

[3.2] T. D. Moustakes, Sol. Energy Mater. **8** (1982) 187.

[3.3] Y. Hamakawa (ed.), JARECT 16, *Amorphous Semiconductor Technologies & Devices,* OHMSAH Ltd. & North-Holland Pub. Co. 1984.

[3.4] B.A. Scott, R.M. Plecenik, and E.E. Simonyi, Appl. Phys. Lett. **39** (1981) 73.

[3.5] A.T. Bell, Solid State Technol. April (1978) 89.

[3.6] P.A. Longeway, in *Preparation and Structure of Hydrogenated Amorphous Silicon,* edited by J. Pankove (Academic, New York, 1984), p.180.

[3.7] G. Turban, Y. Catherine, B. Grolleau, Thin Solid Films, **67** (1980) 309.

[3.8] B. Drevillon, J, Huc, A.Lloret, J. Perrin, G. de Rosny, and J.P.M. Schmitt, Appl. Phys. Lett. **37** (1980) 646.

[3.9] J.P.M. Schmitt, J. Non-Cryst. Solids **59** & **60** (1983) 649.

[3.10] T.Y. Yu, T.M.H. Cheng, V. Kempter, and F.W. Lampe, J. Phys. Chem. **76** (1972) 3321.

[3.11] B.A. Scott, J.A. Reimer, P.A. Longeway, J. Appl. Phys. **54** (1983) 6853.

[3.12] B.A. Scott, M.H. Brodsky, D.C. Green, P.B. Kirby, R.M. Plecenik, and E.E. Simonyi, Appl. Phys. Lett. **37** (1980) 725.

[3.13] J.C. Knights, J. Non-Cryst. Solids **35** & **36** (1980) 159.

[3.14] F.J. Kampas and R.W. Griffith, Appl. Phys. Lett. **39** (1981) 407.

[3.15] P.A. Longeway, R.D. Estes, and H.A. Weakliem, J. Phys.

Chem. **88** (1984) 73.

[3.16] P.A. Longeway, H.A. Weakliem, and R.D. Estes, J. Phys. Chem. **88** (1984) 3282.

[3.17] A. Gallazher, J. Appl. Phys. **63** (1988) 2406.

[3.18] S.R.Mejia, R.D. McLeod, K.C. Kao, and H.C. Card, J. Non-Cryst. Solids **59** & **60** (1983) 727.

[3.19] S.R. Mejia, R.D. McLeod, W. Pries, P. Shufflebotham, D.J. Thomson, J. White, J. Schellenberg, K.C. Kao, and H.C. Card, J. Non-Cryst. Solids **77** & **78** (1985) 765.

[3.20] S.R. Mejia, R.D. McLeod, K.C. Kao, and H.C. Card, Rev. Sci. Instrum. **57** (1986) 493.

[3.21] I. Kato, H.C. Card, K.C. Kao, S.R. Mejia, and L. Chow, Rev. Sci. Instrum. **53** (1982) 214.

[3.22] J.J Schellenberg, R.D. McLeod, S.R. Mejia, H.C. Card, and K.C. Kao, Appl. Phys. Lett. **48** (1986) 163.

[3.23] T.V. Herak, J.J . Schellenberg, P.K. Shufflebotham, and K.C. Kao, J. Appl. Phys. **64** (1988) 688.

[3.24] H. Shanks, C.J. Fang, L. Ley, M. Cardona, F.J. Demond, and S. Kalbitzer, Phys. Status Solidi B, **100** (1980) 43.

[3.25] M.H. Brodsky and P.A. Leary, J. Non-Cryst. Solids **35** & **36** (1980) 487.

[3.26] H. Adachi and K.C. Kao, J. Appl. Phys. **51** (1980) 6326.

[3.27] K.C. Kao, R.D. McLeod, C.H. Leung, H.C. Card, and H. Watanabe, J. Phys. D. **16** (1983) 1801.

CHAPTER IV
EFFECTS OF SUBSTRATE BIAS ON THE PROPERTIES OF a-Si:H FILMS FABRICATED BY ECR PLASMA CVD

4.1 Introduction

Hydrogenated amorphous silicon (a-Si:H) thin films have been extensively studied in the past 15 years and commercially employed for many device applications. In radio-frequency (rf) glow discharge of silane gas, it is difficult to obtain good quality of a-Si:H films at a high deposition rate. In general, good quality films are obtained at high substrate temperature and low rf power. Some new techniques for the fabrication of a-Si:H have been attempted, however they are basically modifications of those conventional deposition methods as mentioned earlier in Chapter III. Among these new fabrication techniques, microwave plasma deposition techniques have been demonstrated to be promising alternatives for the deposition of a-Si:H films [4.1-4.6]. Microwave plasma has been shown to yield high deposition rates [4.7] which are due to the high rates of dissociation as well as ionization of the silane gas, in particular under ECR conditions. Plasma in ECR absorbs microwave power efficiently and results in a more complete gas dissociation since electrons are always accelerated by the microwave electric field for the whole period, resulting in an enhancement of energy transfer. Thus, the plasma maintenance power, operating pressure, and gas temperature can be reduced.

Good quality a-Si:H and μc-Si:H films by microwave plasmas under different deposition conditions have been reported [4.8]. However, the deposition conditions which determine the effects of

radicals and the charged particles bombardment on the growing films have not yet been well understood. It has been shown that the bombardment of charged particles, both ions and electrons, on the growing film is an important factor in determining film properties [4.9,4.10]. The effects of ion bombardment on a-Si:H films deposited by rf glow discharge [4.11,4.12] and multipole dc discharge [4.13-4.15] have been reported. The ion bombardment improves homogeneous growth and film densification. Recently, the effects of a dc bias on films deposited by microwave ECR plasma have been reported [4.16]. Again, the ion bombardment induced by the bias improves the properties of the films. In this chapter we shall present some experimental results on the structural, optical, and electrical properties of a-Si:H films deposited with their surfaces parallel to the magnetic fields in the plasma reactor (waveguide chamber). Comparisons are also made to films deposited on the table with their surfaces normal to the magnetic fields inside the same plasma reactor under a downstream condition.

4.2 Experimental Details

The films were deposited in a ECR microwave plasma CVD system as described earlier in chapter three. Stainless steel and quartz substrates (table samples) were mounted on a thermostatically controlled table which was positioned above the diffusion pump port, with their surfaces normal to the dc magnetic field. Glass substrates (floor samples) were placed on the wall of the waveguide chamber with their surfaces parallel to the magnetic field and perpendicular to the electric field, as shown in Figure 4.1. The table was maintained at a constant potential ranging from -300 to 0 V during deposition. The

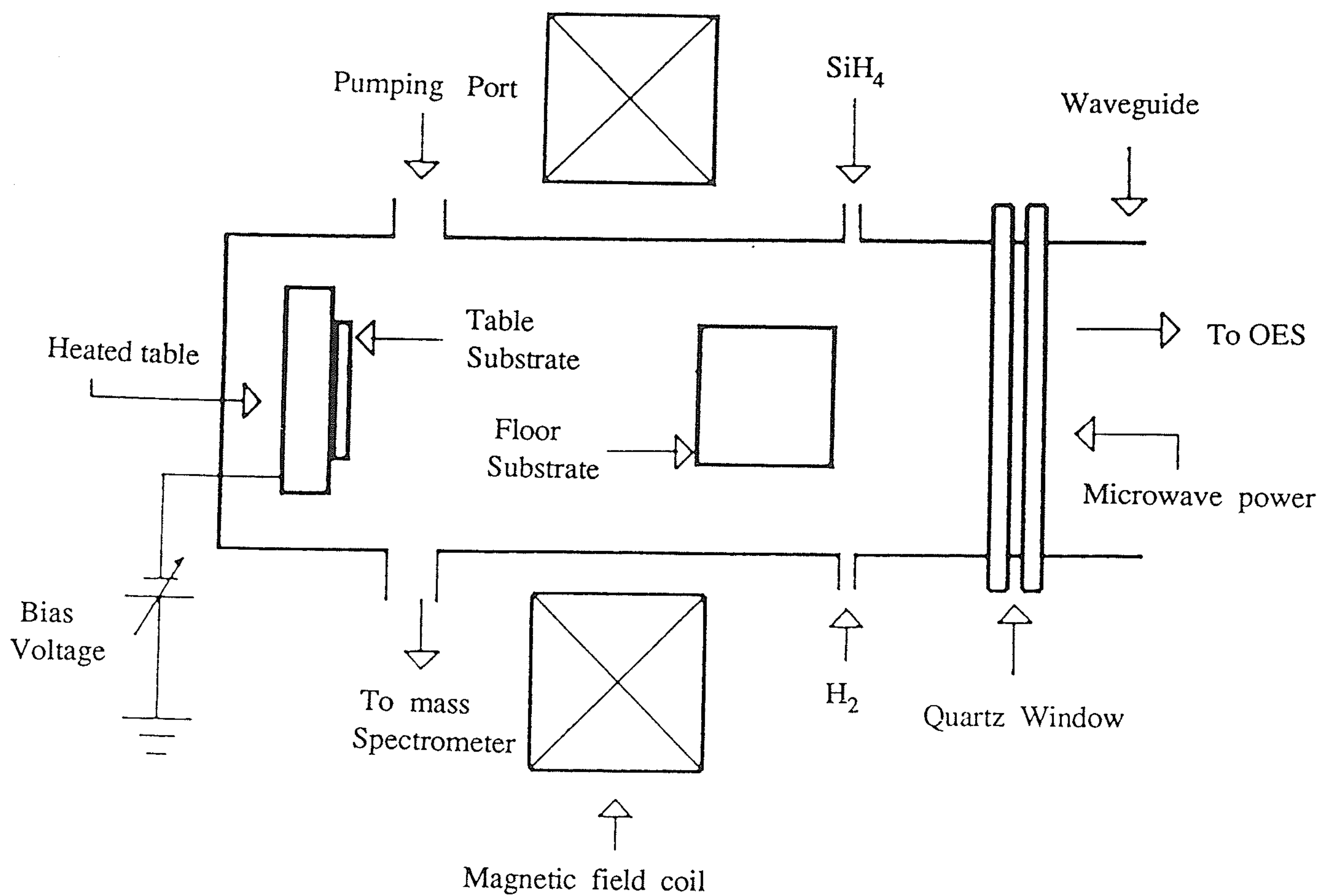

Figure 4.1 Top view of waveguide chamber showing the positions of table and floor substrates.

plasma was maintained at a fixed distance (≈ 10 cm) from the table surface and located between the table and floor samples by adjusting the magnetic field peak position of a single coil. The microwave power was supplied to the chamber through a rectangular waveguide in the TE_{10} mode at the opposite end of the chamber. The chamber was baked at 200^0C and evacuated by a diffusion pump with a cold trap held at liquid nitrogen temperature for 2 hours prior to film deposition. The background pressure of the chamber was better than 10^{-6} Torr. During deposition the chamber temperature was lowered to 160^0C. The plasma was monitored by an optical emission spectrometer and a quadrapole mass spectrometer. A Langmuir probe was also used to determine the plasma parameters as functions of the deposition conditions. Gas flow was controlled with mass flow controllers and chamber pressure was monitored with a capacitance manometer. Film growth was monitored with an *in situ* laser interferometer. Deposition conditions are summarized on Table 4.1.

Table 4.1 Deposition Parameters

Parameter	Value
Background pressure	$\approx 10^{-6}$ Torr
Gas composition	10% SiH_4, 90% H_2
Gas total flow rate	22 sccm
Pressure	10^{-3} Torr
Microwave frequency	2.45 GHz
Microwave power absorbed	4 W
Magnetic field peak	$\approx$ 875 Gauss
Magnetic field strength at sample surface	$\approx$ 275 Gauss
Substrate temperature for Table samples	250°C
Substrate temperature for Floor samples	160°C
Substrates for Table samples	Stainless steel, c-Si, Quartz
Substrates for Floor samples	Glass

The a-Si:H films were characterized with X-ray diffraction, scanning electron microscopy (SEM), Fourier transform infrared spectrophotometry (FTIR), visible and IR spectrophotometry, spectrally resolved ellipsometry, temperature-dependent conductivity and photoconductivity. The results are presented and discussed below.

4.3 Results and Discussions

4.3.1 Film Thickness and X-ray Diffraction

The thickness of the films were measured with a Sloan Dektak mechanical stylus instrument and was confirmed with ellipsometric and near infrared spectrophotometric measurements. The thickness of the a-Si:H films varied from 2.0 to 4.0 μm. All samples deposited were assessed to be amorphous by X-ray diffraction measurements. Figure 4.2 shows a typical X-ray diffraction pattern of the deposited a-Si:H films. The figure indicates that the structure is amorphous. The broad peak at $2\theta \approx 26^{o}$ may be attributed to the short range ordering of the physical structure of the a-Si:H film.

4.3.2 Plasma Parameters

Langmuir probe measurements in a H_2 plasma, as well as in a SiH_4-H_2 plasma, were used to estimate the electron and ion flux energies during film depositions. Figure 4.3 shows the probe I-V characteristics obtained by a planar Langmuir probe located near the table. The floating potential, V_f, can be directly obtained from the figure. It is defined as the voltage where the collected current equals zero, that is, the ion current exactly balances the electron current. This is the voltage which would be assumed by any insulated object inserted into the plasma. Another important plasma parameter is the plasma potential, V_p, which is the self bias assumed by the plasma in order to keep itself quasi-neutral. V_p can be found from the location of the "knee" where the onset of electron current saturation starts. Since our aim of this

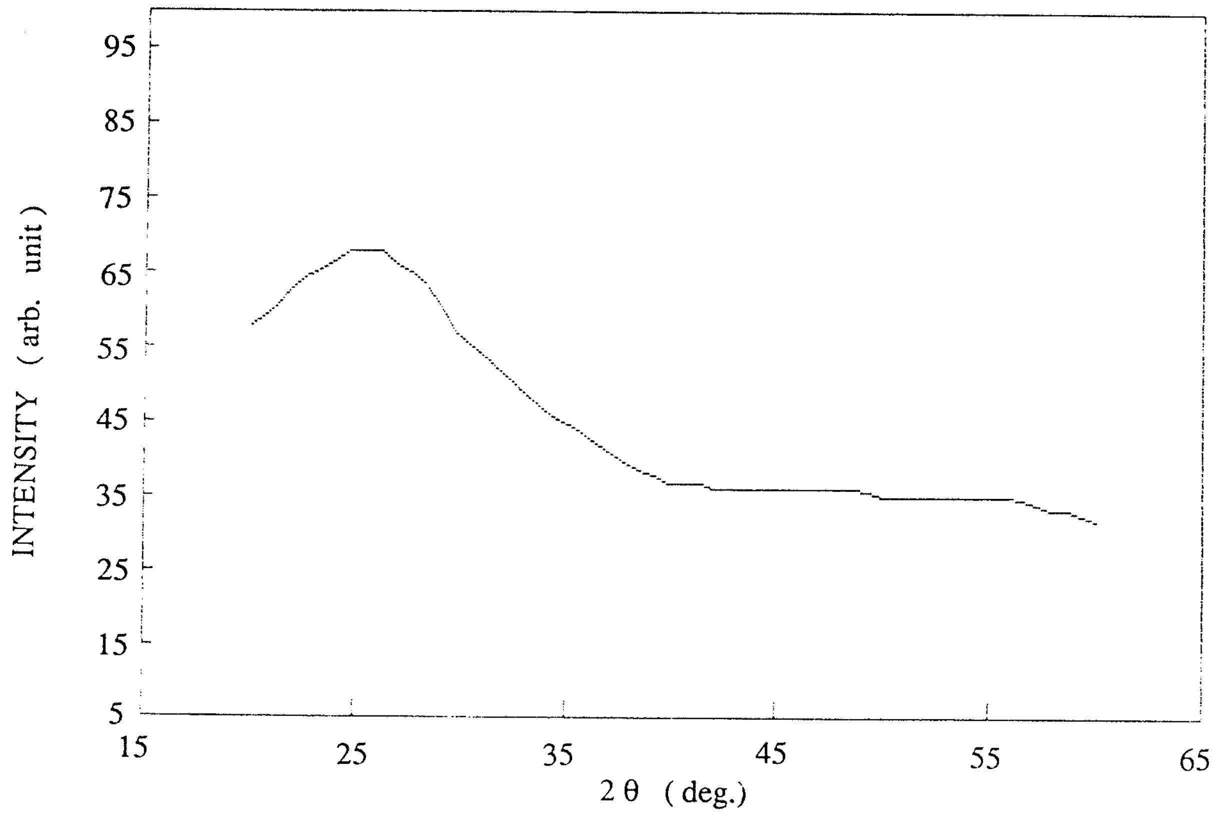

Figure 4.2 Typical X-ray diffraction pattern (Cu-Kα) as a function of scattering angle for a-Si:H films.

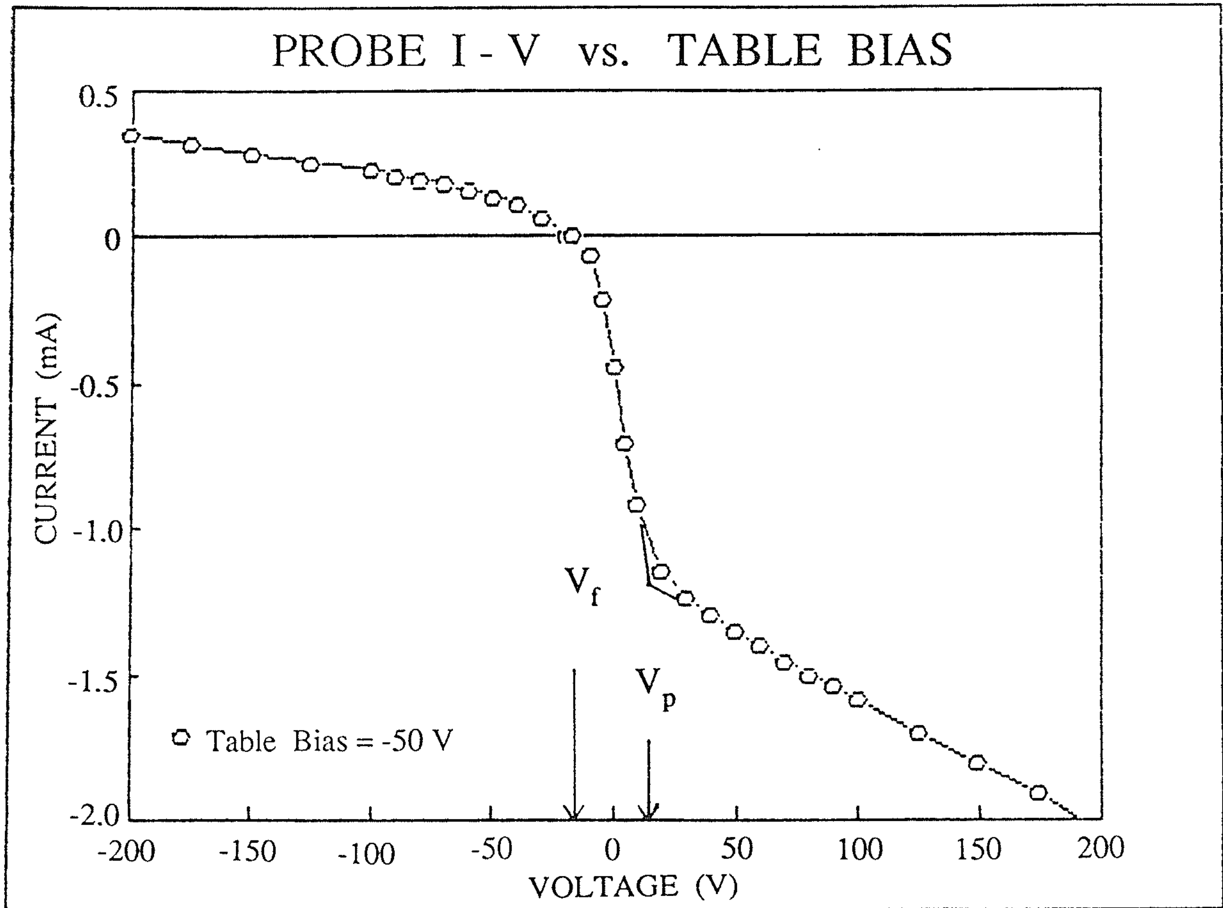

Figure 4.3 Probe I-V characteristic measured by Langmuir plane probe in a H_2 plasma at 1 mTorr with 4 W absorbed microwave power. V_f, the floating potential, and V_p, the plasma potential are also indicated.

research is to study the ion bombardment effects, it is assumed that the mean ion energy impinging on the film surface depends upon the difference between the plasma potential V_p, and the applied substrate potential V_b. It has been shown [4.14] that the mean ion energy in a multipole dc discharge system is given by

$$E_{ion} = e (V_p - V_b) \quad (1)$$

where e is the electronic charge. This is the case for the table samples in which a dc bias is applied. The quartz substrates on the table and glass substrates on the floor are insulating materials and are therefore expected to be negatively self-biased with respect to the plasma reactor walls for a negative potential applied to the table. If they maintain at a floating potential, V_f, the mean ion energy should then be

$$E_{ion} = e (V_p - V_f) \quad (2)$$

Langmuir probe measurements are shown in Figure 4.4, which illustrates the variation in the incident ion energy, E_{ion}, as the table is biased from -300 to 0 V dc in a H_2 plasma. It is assumed that similar trends would be observed in a SiH_4-H_2 plasma . It can be seen that there is little variation in E_{ion} for the insulating substrates, but E_{ion} increases with negative table bias for the conducting substrates..

4.3.3. Deposition Rate and Morphology

The deposition rate, r_d, for all different samples deposited depends on substrate bias as shown in Figure 4.5. For the stainless steel substrates, the deposition state increases initially from 2.25 Å/sec

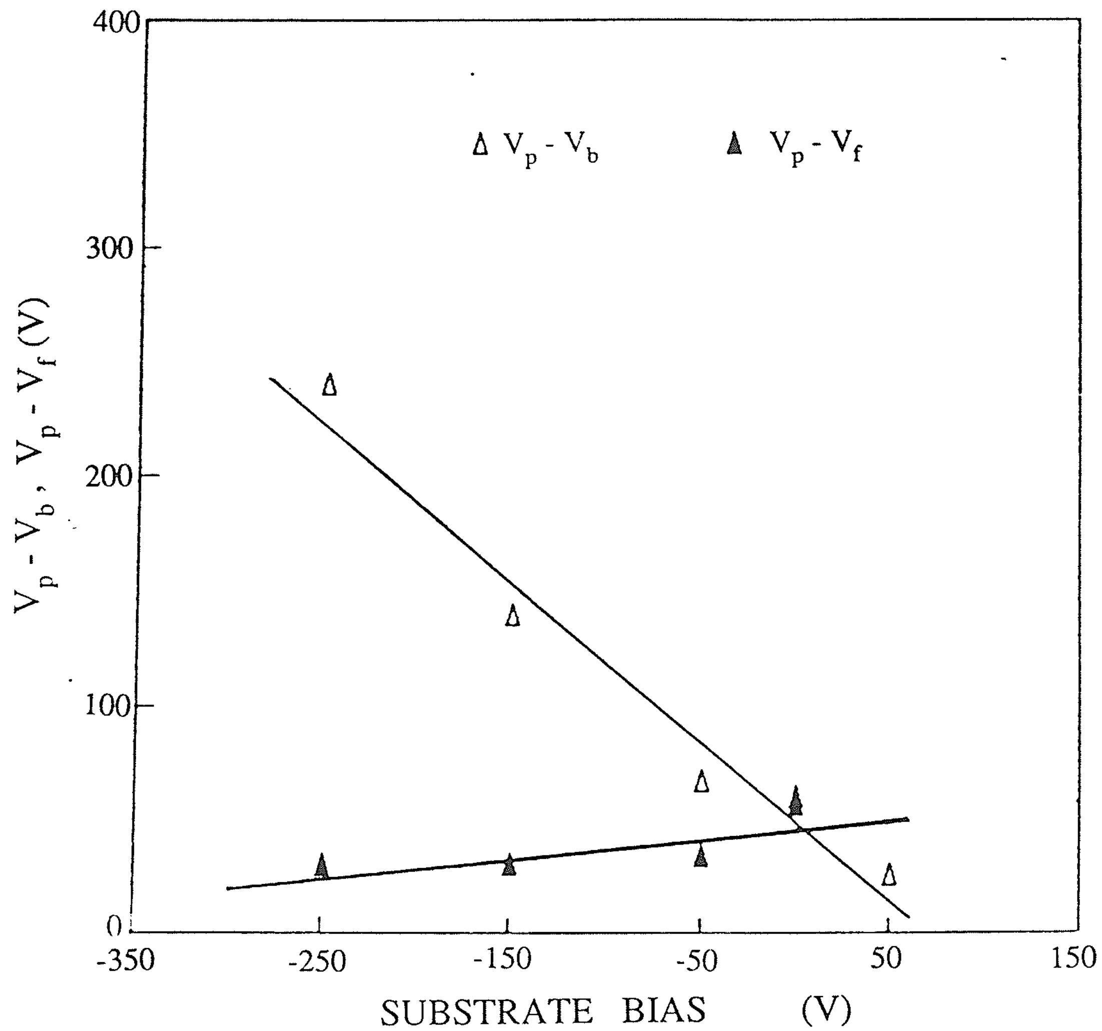

Figure 4.4 The quantities V_p- V_b and V_p-V_f as a function of table bias potential, V_b, as measured by Langmuir probe in a H_2 plasma at 1 mTorr with 4 W absorbed microwave power. (From ref. 4.32)

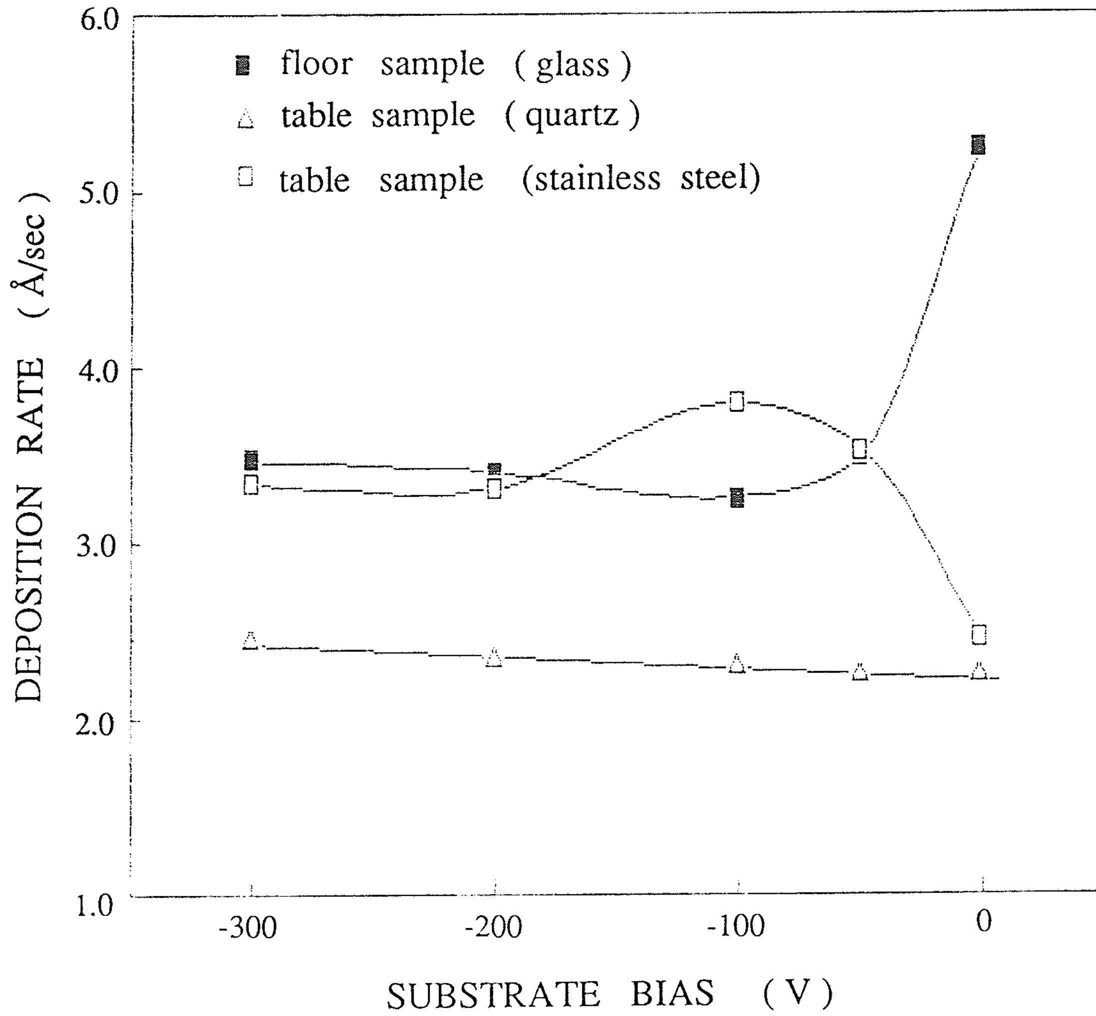

Figure 4.5 Deposition rate of a-Si:H films deposited on the floor and the table as a function of table bias.

at zero bias with an increasing negative bias up to 3.6 Å/sec at V_b = -100 V, and thereafter decreases slightly to 3.3 Å/sec for further increase in negative V_b. This increase in r_d at low E_{ion} (≈ 100 eV) could be attributed to the ion bombardment which may increase the surface reaction rate if this reaction is energy activated [4.16]. Also, the flux of the ions can directly determine the growth kinetics. Assuming that the ions are singly charged and their sticking probability is nearly unity [4.17], the number of silicon atoms deposited per ion has been estimated to be 1-2 in a multipole dc reactor (below 4 mTorr). As a reasonable conjecture, the increased deposition rate could be simply explained by the enhanced transport of ions. Further increases of E_{ion} would reduce the deposition rate due to etching of the growing film surface [4.14]. For the quartz substrates mounted on the same table, the deposition rate is about 2.3 Å/sec, nearly independent of the subsbrate bias V_b as expected.

The deposition rate for the floor samples is 5.25 Å/sec at V_b = 0 V and decreases abruptly to an almost constant value of 3.4 Å/sec with an increasing negative table bias. At V_b = 0 V, the deposition rate of the floor samples is comparatively higher than that of the table samples. This can be due to the position of the substrates. Since the floor samples were placed near the gas inlets where the dissociation of SiH_4 was high and away from the vacuum pump, resulting in a higher deposition rate. As the table is negatively biased, more ions are directed to the table, thus enhancing the deposition rate. Due to the collective behaviour of plasma, substantial amount of electrons are also drawn from the plasma region to the chamber wall to maintain

charge neutrality, this induced electron flow could decrease the dissociation rate of SiH_4 and/or enhance the adatom surface mobility due to heat transfer to the growing surface of the floor samples thereby reducing its deposition rate [4.18]. Here, the term "adatom surface mobility" comes from the condensation process of a film growth model. In such process, incident atoms transfer kinetic energy to the lattice and become loosely bonded "adatoms". These adatoms then diffuse over the surface, exchanging energy with the lattice and other absorbed species, until they become trapped in the lattice sites. Thus, the incorporated atoms can readjust themselves to the favourable positions within the lattice by bulk diffusion process [4.19].

On the other hand, the reduction of the deposition rate could be attributed more or less to the ion bombardment. It is known that ions are more difficult to confine by the magnetic field due to their large mass. Thus, it is possible that some energetic ions, induced by the negative table bias, may run away from the fringe magnetic field lines through sequent collisions. Some of the ions may migrate, or even bombard, to the growing surface of the floor samples, which in turn can cause atomic rearrangement and structural relaxation. This could lead to a better coalescence of the nuclei on the growing film, which would decrease the density deficient overlayer thickness, thus reducing the deposition rate. It has been reported [4.12] that the deposition rate reduces from $r_d = 0.9$ to 0.4 Å/sec as the substrate bias varies from $V_b = 0$ to -150 V, for a-Si:H films fabricated by rf glow discharge.

Samples mounted on the table exhibited smooth fracture surface and no columnar structure, indicating no structural

inhomogeneity and good quality of a-Si:H films. While the floor samples consistently exhibited columnar growth structure; such structural inhomogeneity may be associated with low density and poor photoconductivity. Figure 4.6 shows the scanning electron micrograph of the fracture surface of a floor sample deposited at zero table bias $V_b = 0$ V, and high deposition rate of 5.25 Å/sec. It shows a prominent columnar morphology with columns of 50-170 nm in diameters growing vertically from the substrate.

In conventional rf glow discharge system, this columnar growth morphology can be suppressed by suitable deposition conditions, such as, low deposition rates (≤ 2 Å/sec), higher SiH_4 concentration and larger negative biases of the substrate with respect to the plasma potential [4.19,4.21,4.22]. Since an a-Si:H film is considered to be composed of a grain-like (GL) region and a grain-boundary like (GBL) region [4.23], we can recognize the GL region as in the column and the GBL region as in the intercolumn. It is tempting to speculate that the ion bombardment on the table sample could enhance the smoothing of the fracture surface and thus suppress the columnar growth structure, that is, an increase in the GL region and a decrease in the GBL region [4.19]. This enhancement would in turn lead to a better film quality with a high density and photoconductivity. For the floor samples, on the other hand, we speculate that either the induced electron flow or the "runaway" ions by the negative table bias would also suppress, to some extent, the GBL region and cause a slight increase in the film's density. This will be seen from the increase of refractive index and photoconductivity in the following sections.

Infrared absorption measurements of the films deposited on

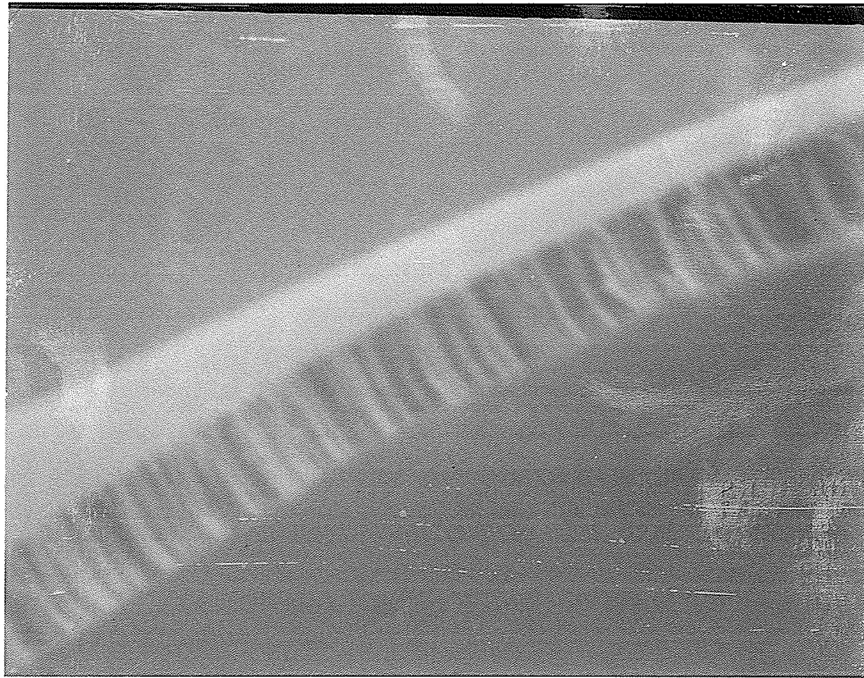

Figure 4.6 Scanning electron micrograph of the fracture surface of a-Si:H film (floor sample) deposited at a table bias $V_b = 0$, illustrating the columnar structure.

the table with negative bias show a single peak at 2000 cm^{-1} corresponding to the Si-H stretching modes. Figure 4.7 shows the IR absorption spectrum for a table sample deposited with negative table bias, V_b = -100 V. Absorptions near 2100 cm^{-1} and 1050 cm^{-1} have not been observed indicating the absence of Si=H_2 and Si-0 bonds. All H is incorporated solely in a mono-atomic, singly bonded form. The total bonded hydrogen content has been estimated to be about 6 at.%. These properties are usually displayed by high density and good quality of a-Si:H films. The floor samples consistently exhibiting columnar structure and low density, as mentioned earlier, are expected to have hydrogen incorporated in both Si-H and Si=H_2 bond configurations as reported in previous studies [4.8]. This can be attributed mainly to the lack of ion bombardment during film growth. Since the scouring action of ionic species on the film surface during growth seems responsible for elimination of H bonded as Si=H_2 [4.22]. Furthermore, these samples are unstable upon exposure to atmosphere. The interstitial regions between the columns can be penetrated by active atmospheric impurities, such as CO_2, N_2, O_2, leading to post-deposition contamination effects. Thus, the electronic properties are expected to be poor since the interstitial regions are correlated with electronically active defects [4.21, 4.24] .

4.3.4 Optical Properties

The results of refractive index, n, for the floor samples and the table samples as a function of photon energy are shown in Figure 4.8 and Figure 4.9. For both samples, a broad peak occurs at ≈ 2.5 eV

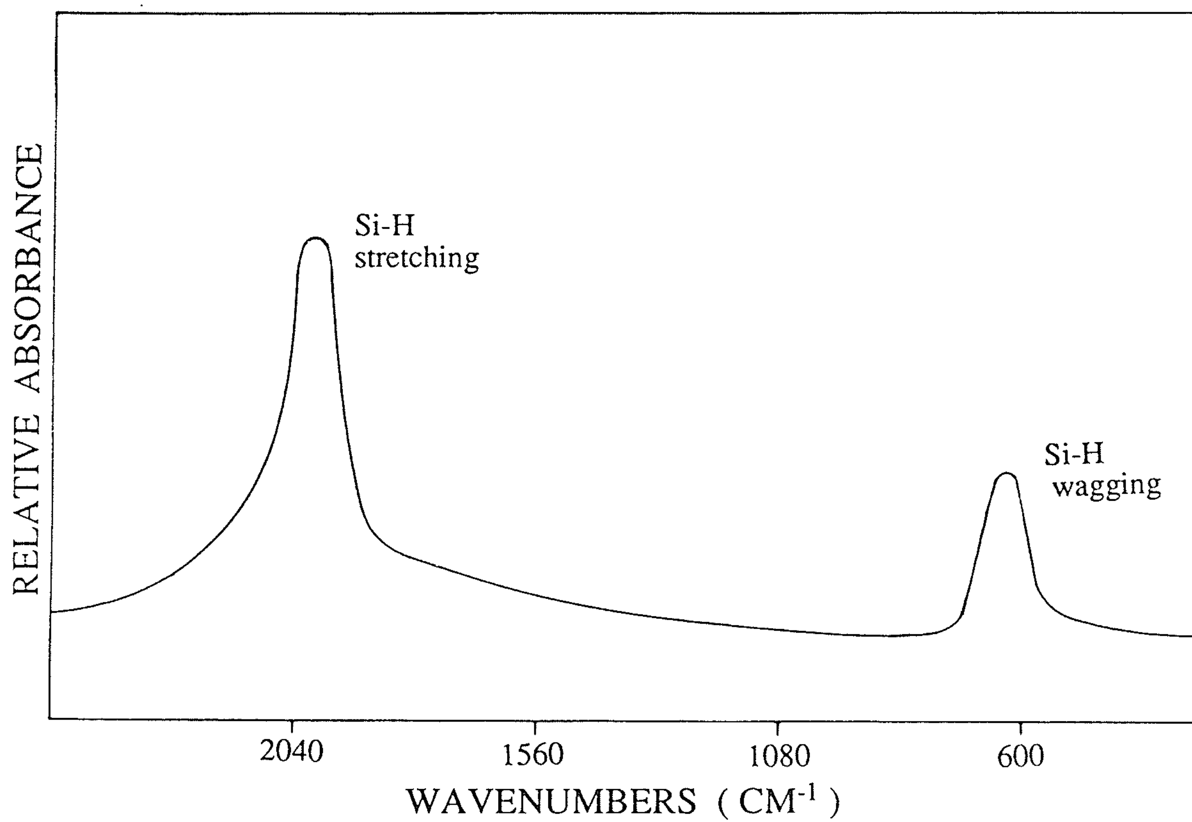

Figure 4.7 IR absorption spectrum of a table sample with table bias, V_b = -100 V. Absorption bands for monohydride are stretching and wagging modes.

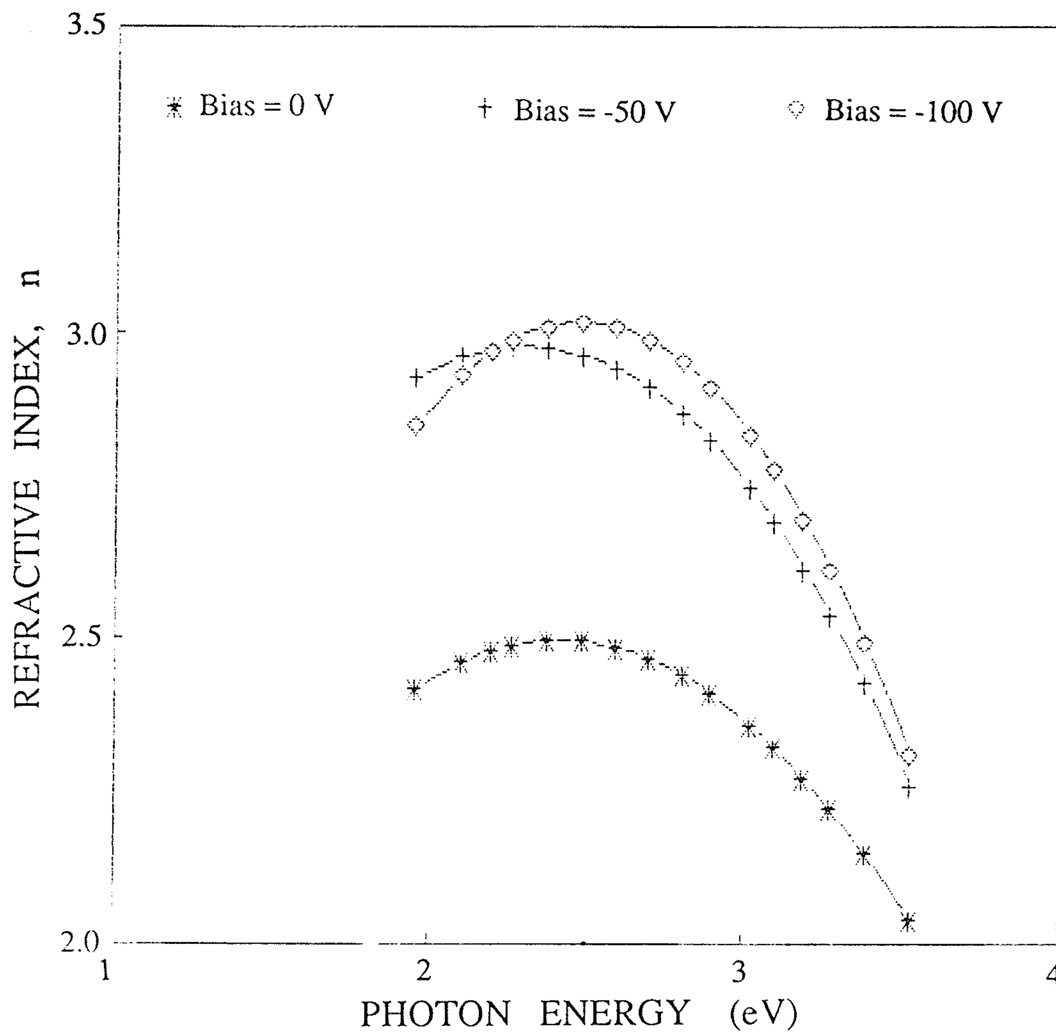

Figure 4.8 The refractive index, n, as a function of photon energy for a-Si:H films deposited on glass substrates, i.e., floor samples, for various table bias, V_b.

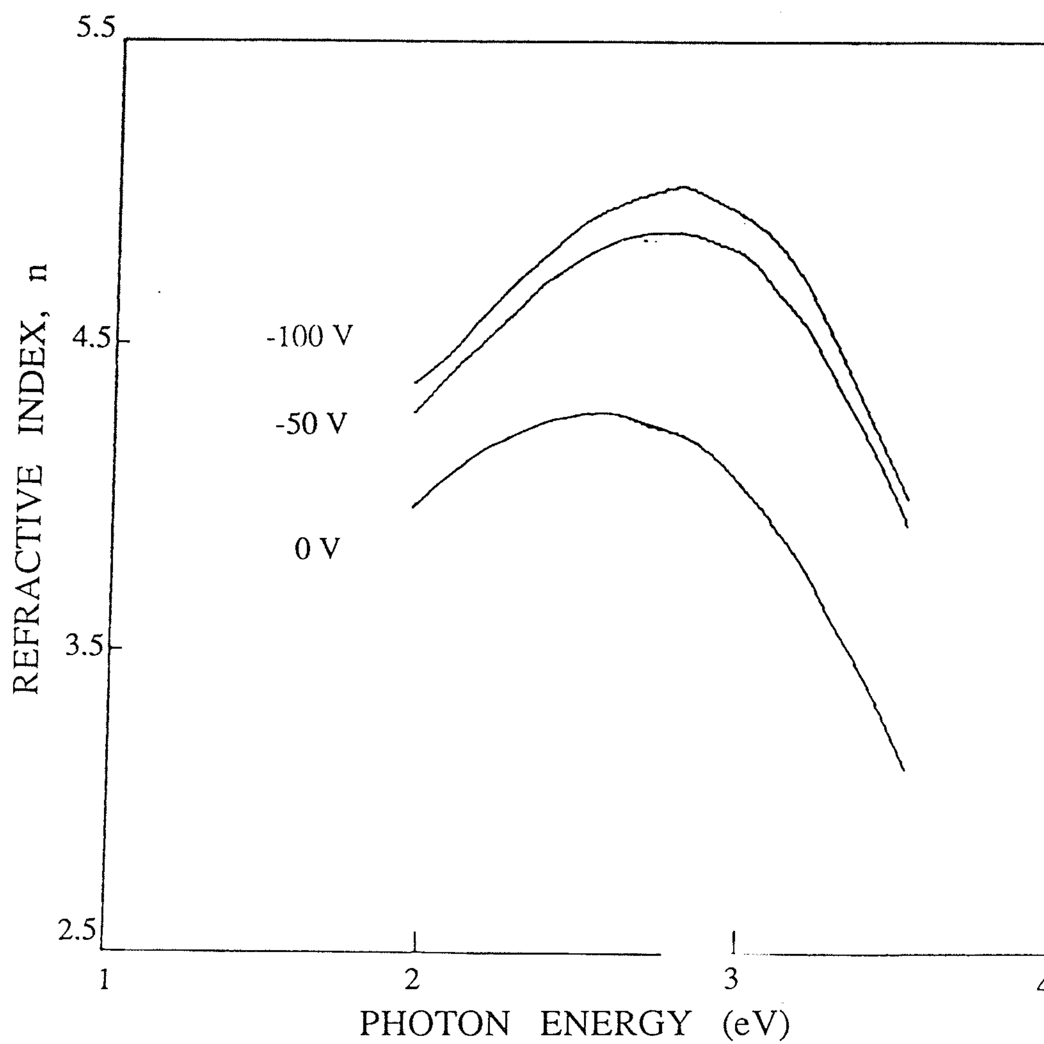

Figure 4.9 The refractive index, n, as a function of photon energy for a-Si:H films deposited on stainless steel substrates, i.e., table samples, for various table bias, V_b. (From ref. 4.32)

in all the refractive index spectrum as is usually observed for amorphous silicon films. The n spectrum of both table and floor samples films deposited with table bias, V_b < -100 V shows no significant differences as compared to V_b = -100 V. The n spectrum of the floor samples, prepared at table bias V_b = -100 V, has a limiting peak value of ≈ 3, while the corresponding peak value of the table samples is ≈ 5. This indicates that the table samples have a higher density since n depends on the density of the valence electrons, as given in References 4.33, 4.34. It is noted that the n spectra for both samples are enhanced by increasing negative table bias.

Figures 4.10 and 4.11 show the imaginary part of the dielectric constant, ε_2, as a function of photon energy for the floor samples and the table samples, respectively. Each of these ε_2 spectra can be characterized by its maximum of value, $\varepsilon_{2\,max}$, and its position. The relatively low value of the maximum of $\varepsilon_2 \approx 8$ for the floor samples can be related to the low density of the material. On the other hand, the high value of $\varepsilon_{2\,max} \approx 28$ of the table samples corresponds to high density a-Si:H films. The position of the ε_{2max}, for both samples, does not appear to be significantly affected by the table bias V_b. This implies that the surface roughness of all samples is not affected by the table bias [4.26, 4.27].

Figure 4.12 shows the maximum value of the ε_2 spectra, ε_{2max}, as a function of substrate bias for all deposited samples. It is noted that the table samples consistently demonstrate a higher value of

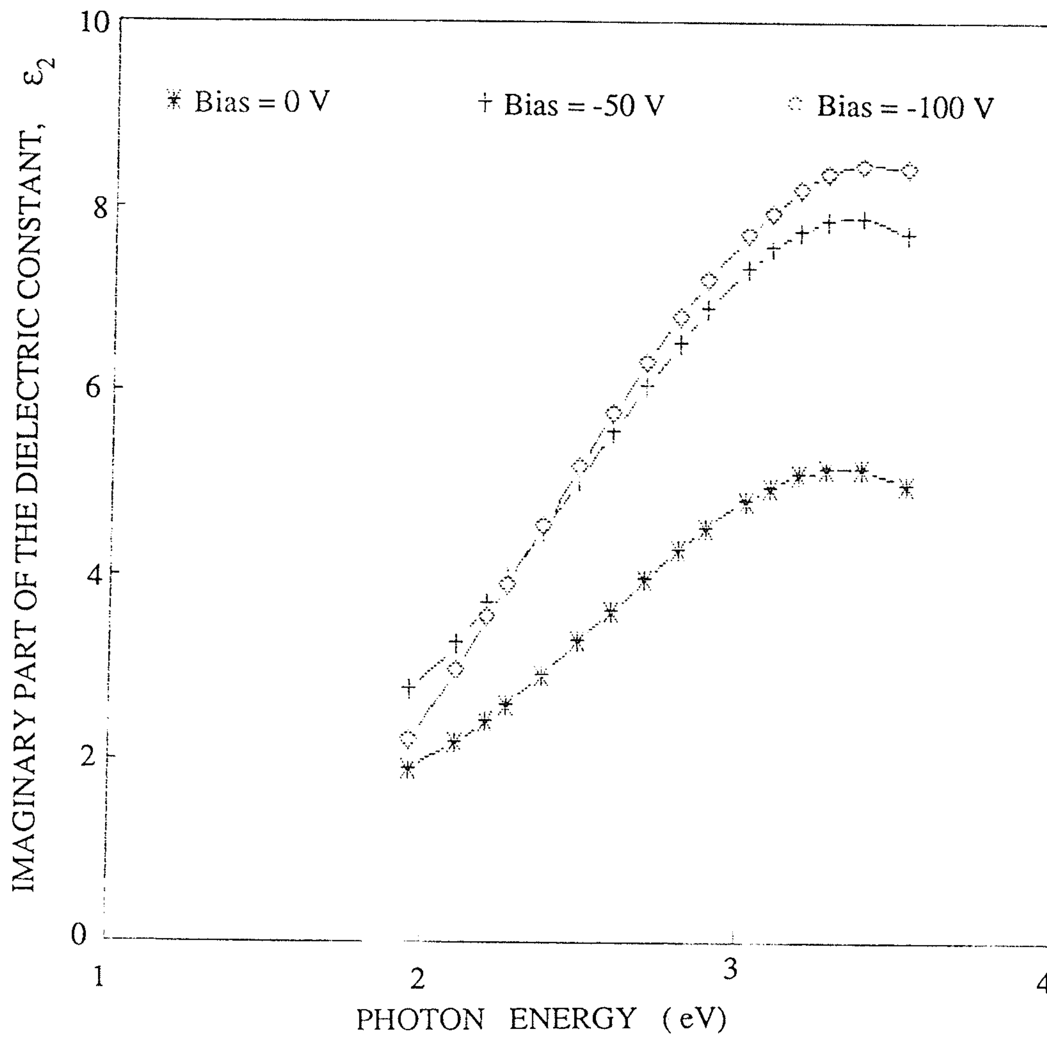

Figure 4.10 The imaginary part of the dielectric constant, ε_2, as a function of photon energy for a-Si:H films deposited on glass substrates (floor samples).

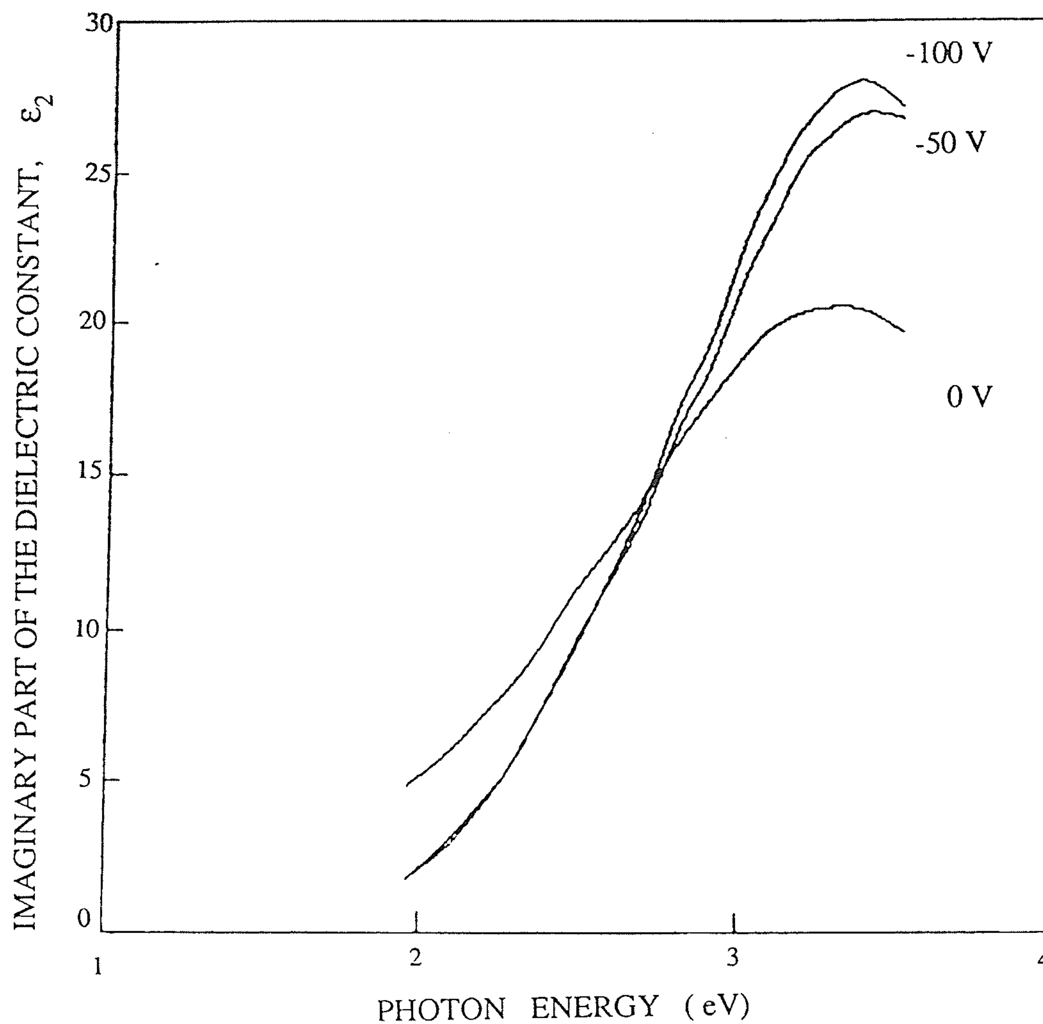

Figure 4.11 The imaginary part of the dielectric constant, ε_2, as a function of photon energy for a-Si:H films deposited on stainless steel substrates (table samples). (From ref. 4.32)

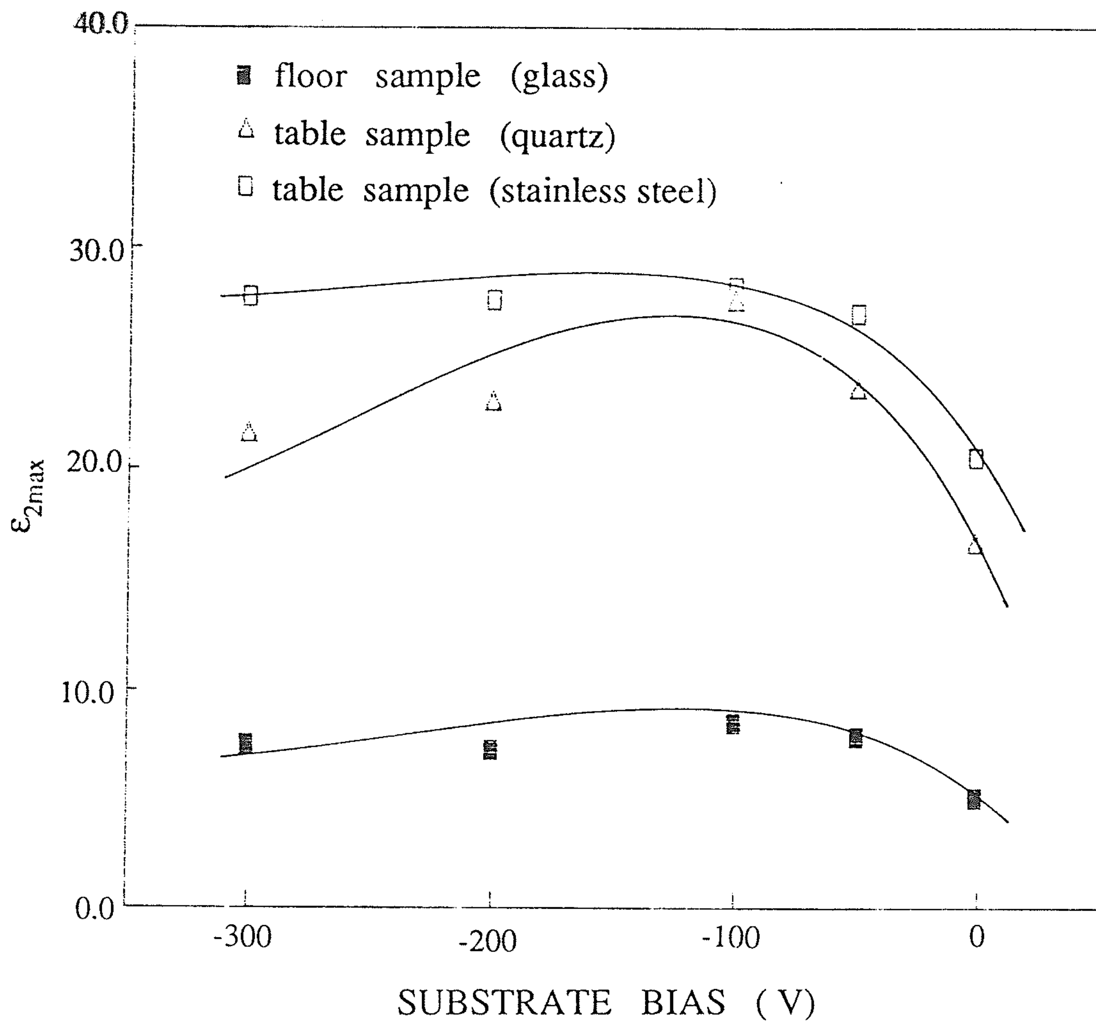

Figure 4.12 The maximum value of the imaginary part of the dielectric constant, ε_{2max}, as a function of table bias, V_b, for a-Si:H films deposited on glass, quartz, and stainless steel substrates.

ε_{2max} as compared to the floor samples. These results can be explained as follows. Firstly, the higher value of ε_{2max} with a higher substrate temperature is usually observed in a-Si:H films prepared from glow discharge [4.26]. Secondly, the ion bombardment during film growth is the main parameter controlling the film structural homogeneity, that is, the ion bombardment results in the film densification [4.14,4.15]. Since the floor samples were held with their surfaces parallel to the fringing magnetic field line, ion bombardment was not expected during film growth because of the magnetic screening effect, resulting in a density deficient and inhomogeneous growth in the material. Moreover, the results illustrated in Figure 4.12 show that ε_{2max} of the table samples, both stainless steel and quartz substrates, increase on the range V_b = 0 to -100 V, then decrease slightly at higher values of V_b. This can be inferred that moderate energy ion bombardment, follows Eqn. (1)-(2), induces a very efficient heating on the substrate which in turn enhances the surface mobility of the reactive ion species, thus resulting in an increase in density of the material.

For the floor samples ion bombardment was not expected to occur. However, the "runaway" ions which migrate down to the floor substrates could still be responsible for the increase of ε_{2max} by increasing the density of the film through a weak momentum transfer. On the other hand, the increase of ε_{2max} could also be attributed to the electron flow to the floor substrates since the floor substrates were always negatively self biased with respect to the plasma chamber wall and electrons would have a much higher mobility than ions at 1

mTorr. Also, the electron arriving at the floor substrates is enhanced due to the collective behaviour of the plasma as the table is negatively biased. Thus, it is possible that the effect of electron flow may cause the surface heating and in turn enhance adatom surface mobility, leading to a slight improvement in density of the films.

Assuming parabolic bands, the optical gap E_{opt} is defined by [4.29]

$$\alpha h\nu = B(h\nu - E_{opt})^2 \qquad (3)$$

where α is absorption coefficient and $h\nu$ is photon energy. Figure 4.13 shows the absorption coefficient of the floor sample as a function of table bias. The absorption coefficient is slightly enhanced by negative table bias. Figure 4.14 shows the optical gaps E_{opt} of the table samples and the floor samples as a function of table bias. The optical gap of the stainless steel table samples initially increases with negative substrate bias up to V_b = -100 V, thereafter remaining unaffected. The same tendency is also observed for the floor samples.

The variation of the optical gaps seems to have the same manner as ε_{2max}, as shown in Figure 4.12, that is E_{opt} increases with increasing ε_{2max}. This implies that E_{opt} is also associated with the density of the film. The E_{opt} of the floor samples are relatively low due to low density and less amount of hydrogen content, since a large E_{opt} is associated with the amount of hydrogen. This is probably caused by lack of ion bombardment (H^+, $Si_nH_m{}^+$) during film growth.

The parameter B in Eqn. (3) has been used as a characterization parameter for amorphous materials [4.29]. This value

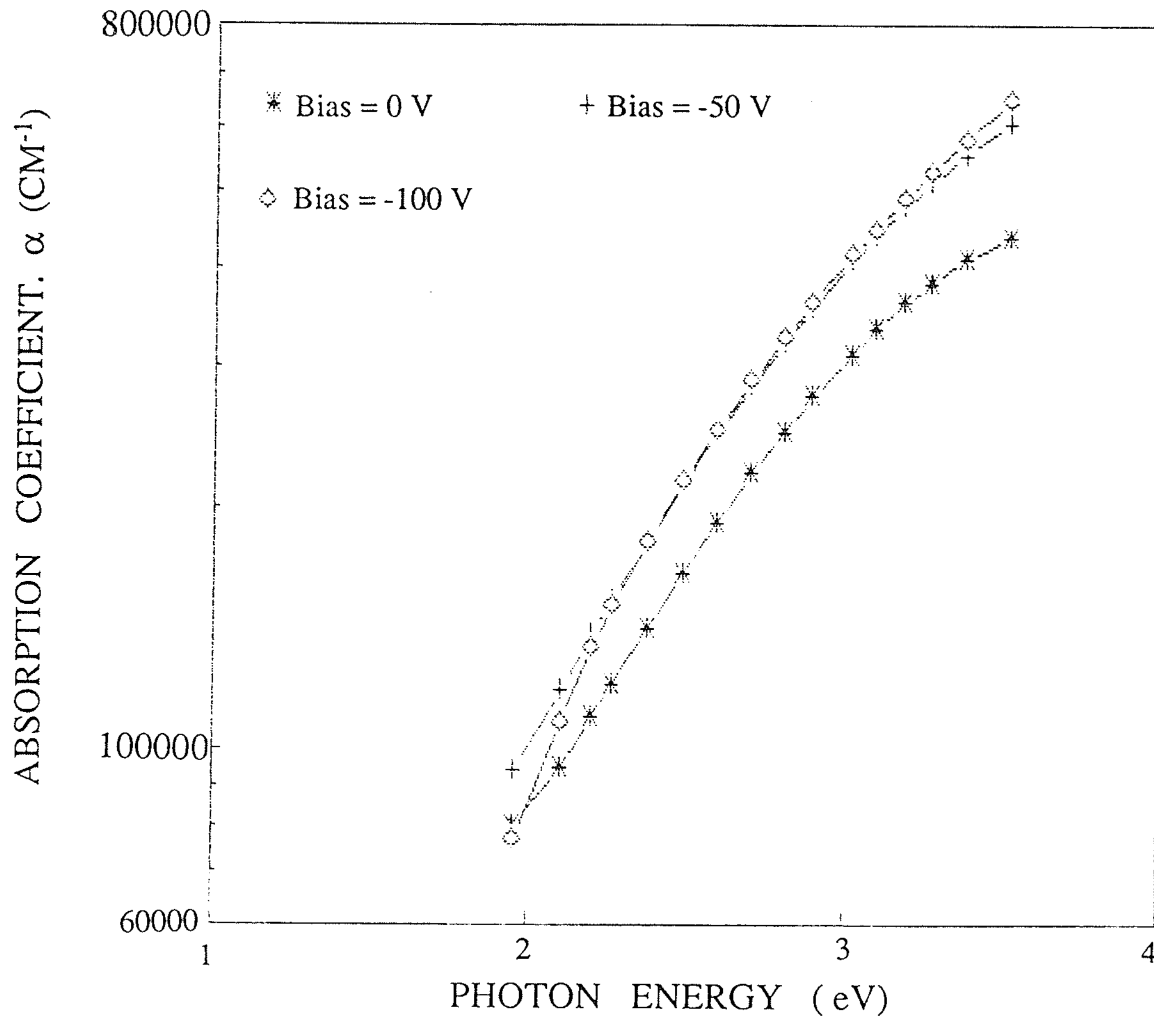

Figure 4.13 Optical absorption coefficient as a function of photon energy for a-Si:H films deposited on glass substrates (floor samples) for various table bias, V_b.

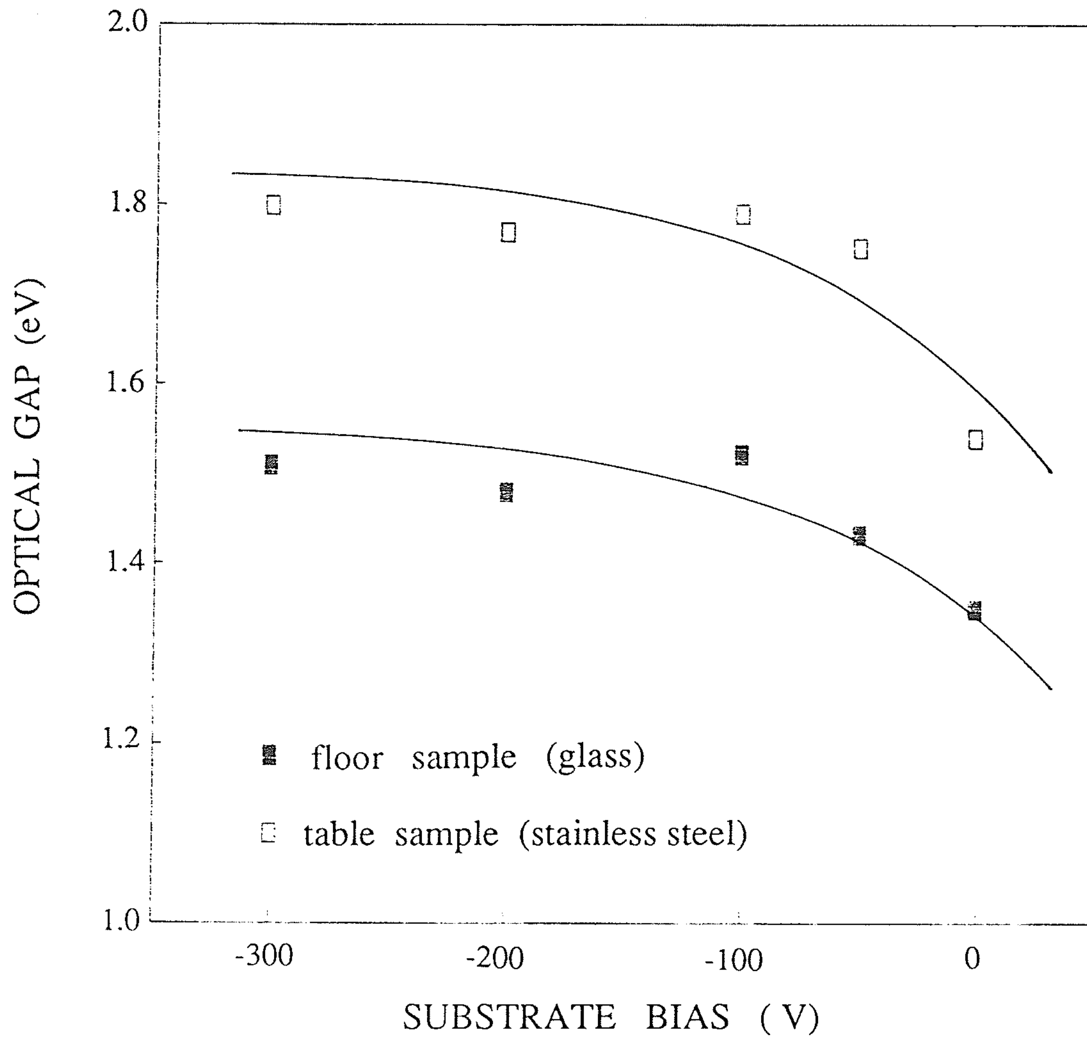

Figure 4.14 Optical gap E_{opt} as a function of table bias, V_b, for a-Si:H films deposited on stainless steel substrates (table samples) and glass substrates (floor samples).

is inversely proportional to the width of the tail states and reflects the steepness of the state density rise at the conduction band edge [4.30]. Therefore, this parameter is related to the quality of a-Si:H films [4.29]. Figure 4.15 shows the dependence of B-parameter on the substrate bias for both samples. The B-parameter has the same tendency as E_{opt} , with maximum value occurring at V_b = -100 V. This implies that the extent of the tail states at the edges decreases with ion energy up to 100 eV for film deposited on stainless steel substrates on the table. On the other hand, the induced electron flow by the moderate negative bias also suppresses the extent of the tail states at the conduction band edge, resulting in a better quality material.

4.3.5 Electrical Properties

Figure 4.16 shows the dark conductivity and photoconductivity, at room temperature, as function of the table bias for the floor samples. For films deposited under negative table bias the dark conductivity is on the order of 10^{-9} ($\Omega^{-1}.cm^{-1}$). In the high temperature range, the transport is dominated by extended state conduction with activation energies ranging from 0.65 to 0.9 eV as the table is negatively biased from 0 to -300 V. The variation of the activation energy seems to have the same manner as the optical gap and ε_{2max}. Since the films exhibit columnar morphology, the photoconductivity is only on the order of 10^{-7} ($\Omega^{-1}.cm^{-1}$) under negative table bias. However, the film deposited at a V_b = -100 V has a high photoconductivity of $1.5x10^{-6}$ ($\Omega^{-1}.cm^{-1}$). The increase of photoconductivity could be attributed to the decrease of the gap state density due to the increase of the Si-H content and/or the increase of

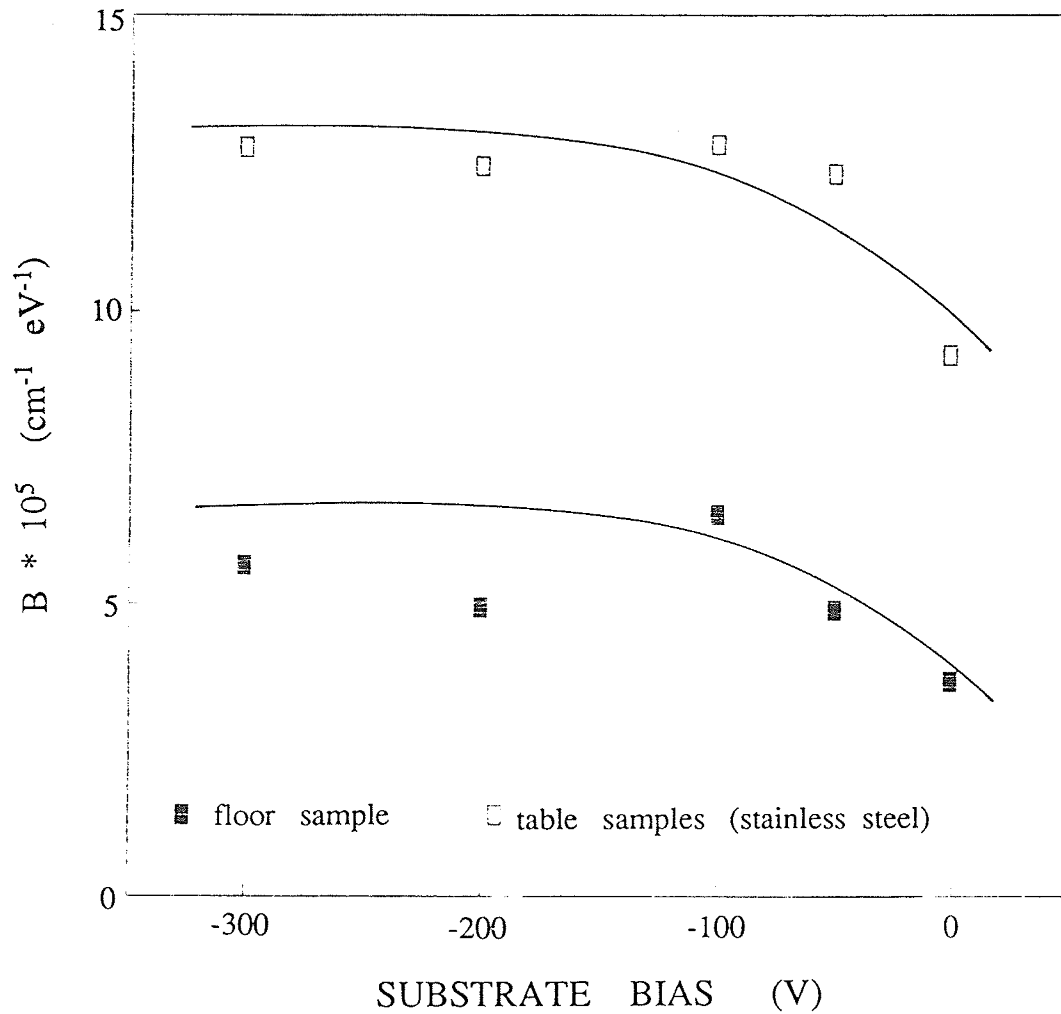

Figure 4.15 The B-parameter of the Tauc's plot as a function of table bias, V_b, for a-Si:H films deposited on stainless steel substrates (table samples) and glass substrates (floor samples).

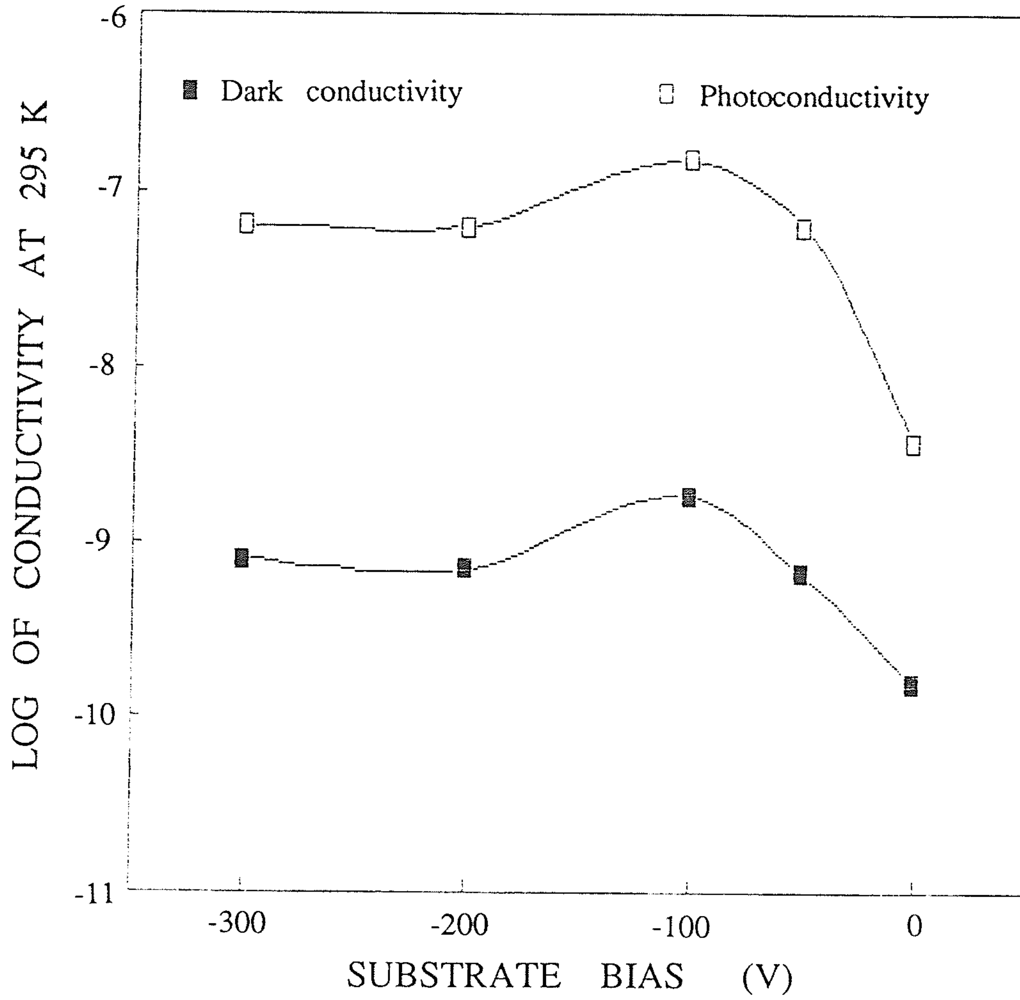

Figure 4.16 Dark conductivity and photoconductivity at room temperature as functions of table bias for a-Si:H films deposited on glass substrates (floor samples).

GL regions, since both the optical gap and the refractive index increase with the negative table bias.

The dark conductivity and the ratio of photoconductivity to dark conductivity as functions of the table bias for both floor samples and table samples are shown in Figures 4.17 and 4.18, respectively. The floor samples increase from one order to two order of magnitude in the conductivity ratio, indicating an improvement in film quality with negative table bias. On the other hand, the table samples display high photoconductivities typical of good quality films.

In general, films with good optical properties also exhibit good electronic properties. Figure 4.19 shows the correlation between photoconductivity and B-parameter of the Tauc's plot. It is clear that films with large value of B also display large value of photoconductivities. This correlation is not yet well understood since B is mainly related to the tail states, while photoconductivity is related to the gap states. However, this observed correlation may suggest that the origins of the tail states and gap states are related to each other.

At this point we have demonstrated that high density, good optical and electrical properties of a-Si:H films can be produced with some ion bombardment in ECR microwave plasma, as is the case of the table samples. We have also shown, from the observed structural, optical and electrical properties of the floor samples, that negative table bias potential can cause significant changes in the plasma as well as film's quality. However, it is difficult at this stage to differentiate the relative roles and the existences of electron flow or "runaway" ions in the growth of the film because of insufficient experimental results. Moustakas [4.31] has reported the dependence of the substrate

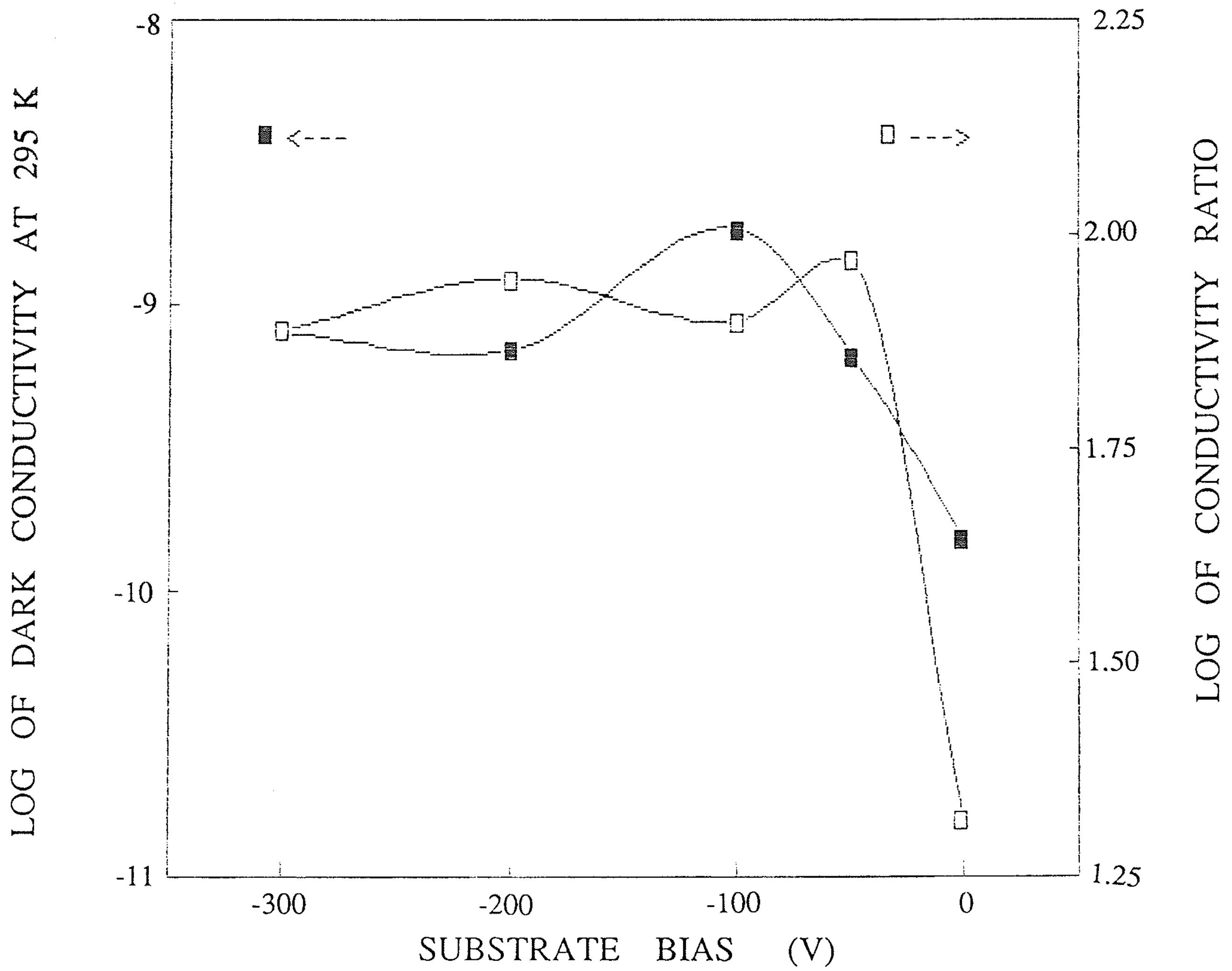

Figure 4.17 Dark conductivity and the ratio of photo- to dark conductivity as functions of table bias for a-Si:H films deposited on glass substrate (floor samples).

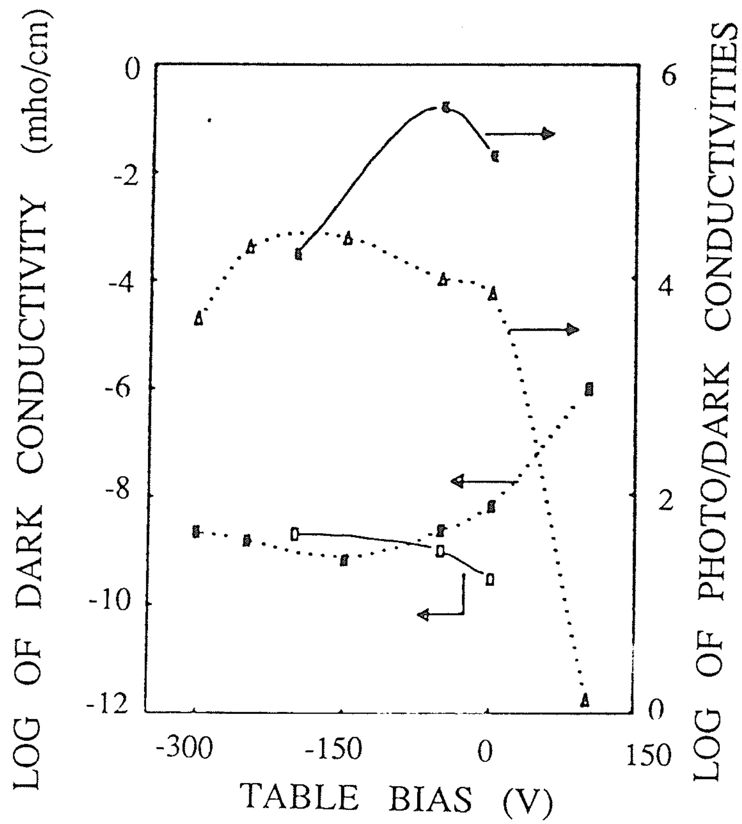

Figure 4.18 Dark conductivity and the ratio of photo- to dark conductivity as functions of table bias for a-Si:H films deposited on stainless steel (solid line) and quartz (dotted line) substrates. (From ref. 4.16)

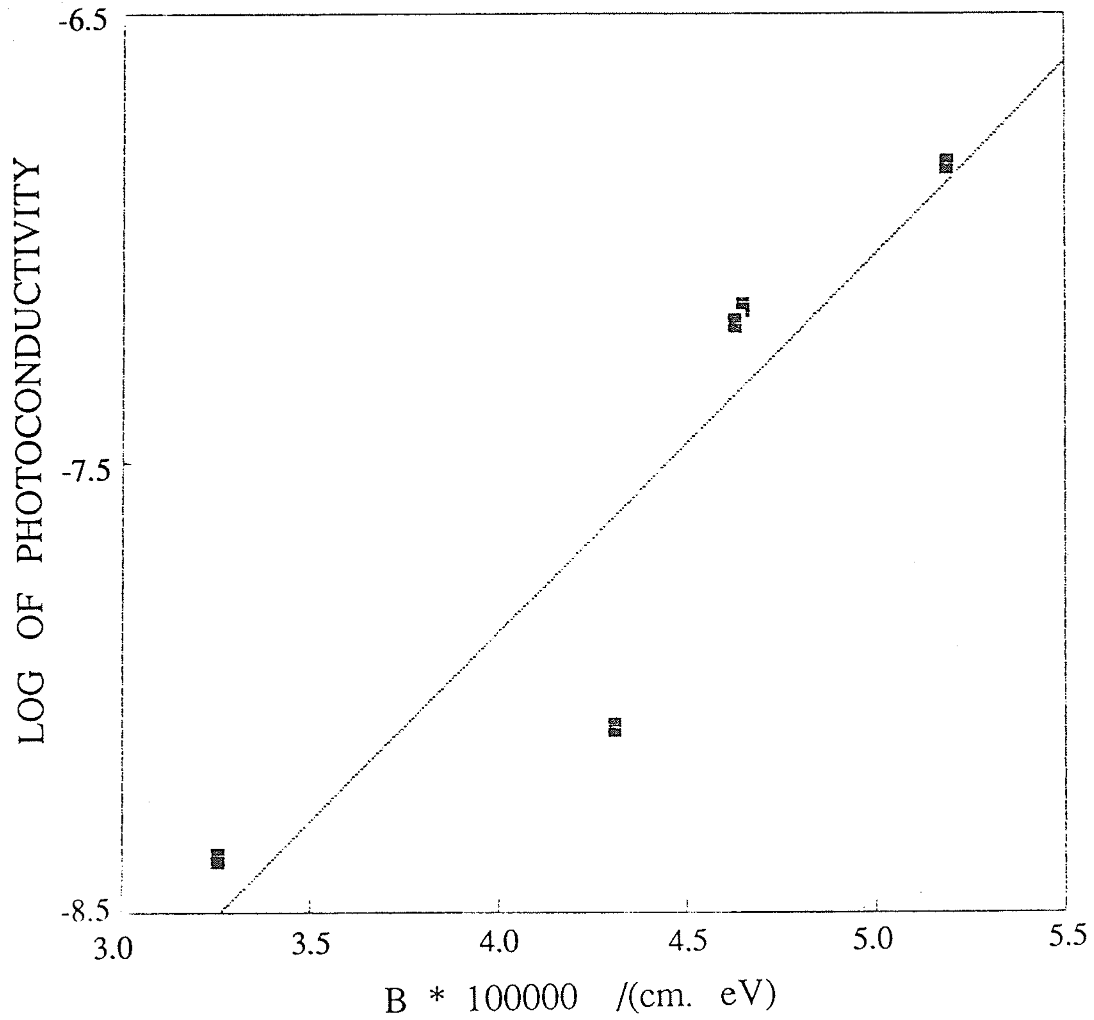

Figure 4.19 Correlation between photoconductivity and *B*-parameter of the Tauc's plot for a-Si:H films deposited on glass substrates (floor samples).

self-bias voltage on the gas pressure for rf sputtered a-Si:H films in H_2-Ar mixtures. He has obtained negative self-bias potentials at low pressures ($\leq$ 15 mTorr) and small argon contents. He has proposed that the negative self-bias are due to electron bombardment which enhances the adatom surface mobility through surface heating, resulting in structural and compositional homogeneous films. It has also been reported [4.18] that the adatom mobility could lead to a better coalescence in the columnar structure. In our case we speculate that the improved properties of the floor samples due to table bias could be attributed to the electron flow on the growing films.

4.4 Conclusions

In conclusion, this study has demonstrated that some ion bombardment during film growth is responsible for film densification and reduction of dihydrides. It has also demonstrated that films deposited with a low substrate temperature and lack of ion bombardment exhibit low density, columnar growth morphology, and poor optical and electrical properties. However, we can conclude that some electrons arriving at the substrates can have a favourable effect on the film's structure and properties, as is the case of the floor samples. It is believed that this electron flow is responsible for enhancing the coalescence of the island structure and leading to a better film quality.

References

[4.1] I. Kato, S. Wakana, S. Hara and H. Kezuka, Jpn. J. Appl. Phys. **21** (1982) L470.

[4.2] S. Matsuo and M. Kiuchi, Jpn. J. Appl. Phys. **22** (1983) L210.

[4.3] S. Kato and T. Aoki, J. Non-Cryst. Solids, **77** & **78** (1985) 813.

[4.4] L. Paquin, D. Masson, M.R. Wertheimer, and M. Moisau, Can. J. Phys. **63**, (1985) 831.

[4.5] K. Kobayashi, M. Hayama, S. Kawamoto, and H. Miki, Jpn. J. Appl. Phys. **26** (1987) 202.

[4.6] M. Hayama, K. Kobayashi, S. Kawamoto, H. Miki, and Y. Onishi, J. Non-Cryst. Solids. **97** & **98** (1987) 273.

[4.7] S.R. Mejia, R.D. McLeod, K.C. Kao, and H.C. Card, J. Non-Cryst. Solids **59** & **60** (1983) 727.

[4.8] S.R. Mejia, R.D. McLeod, W. Pries, P. Shufflebotham, D.J. Thomson, J. White, J. Schellenberg, K.C. Kao, and H.C. Card, J. Non-Cryst. Solids **77** & **78** (1985) 765.

[4.9] D.J. Ball, J. Appl. Phys., **43** (1972) 3047.

[4.10] J.J. Hanak and J.P. Pellicane, J. Vac. Sci. Technol.**13** (1976) 406.

[4.11] A.M. Antoine, B. Drevillon, and P. Roca I Cabarrocas, J. Non-Cryst. Soilds, **77** & **78** (1985) 769.

[4.12] A.M. Antoine, B. Drevillon, and P. Roca I Cabarrocas, J. Appl. Phys. **61** (1987) 2501.

[4.13] K. Ando, M. Aozasa, and R.G. Pyon, Appl. Phys. Lett. **44** (1984) 413.

[4.14] B. Drevillon, J. Perrin, J.M. Siefert, J. Huc, A. Lloret, G. de Rosny, and J.P.M. Schmitt, Appl. Phys. Lett. **42** (1983) 801.

[4.15] B. Drevillon, J. Huc, and N. Boussarssar, J. Non-Cryst. Solids **59** & **60** (1983) 735.

[4.16] T.V. Herak, T.T Chau, S.R. Mejia, P.K. Shufflebotham, J.J. Schellenberg, H.C. Card, K.C. Kao, and R.D. McLeod, J. Non-Cryst. Solids **97** & **98** (1987) 277.

[4.17] J.P.M. Schmitt, J. Non-Cryst. Solids **59** & **60** (1983) 6489.

[4.18] Gy. Zentai and L. Pogany, Thin Solid Films **116** (1984) 251.

[4.19] R.G. Pyon, M. Aozasa, and K. Ando, Jpn. J. Appl. Phys. **25** (1986) 944.

[4.20] J.A. Thornton, Ann. Rev. Mater. Sci. **7** (1977) 239.

[4.21] J.C. Knights, G. Lucovsky, and R.J. Nemanich, J. Non-Cryst. Solids **32** (1979) 393.

[4.22] J.C. Knights, J. Non-Cryst. Solids **35** & **36** (1980) 159.

[4.23] H. Fritzsche, Sol. Energy Mater. **3** (1980) 447.

[4.24] J.C. Knights, R.A. Lujan, M.P. Rosenblum, R.A. Street, and D.K. Biegelson, Appl. Phys. Lett. **38** (1981) 331.

[4.25] J.C. Knights and R.A. Lujan, Appl. Phys. Lett. **35** (1979) 244.

[4.26] D. Ewald, M. Milleville, and G. Weiser, Philos. Mag. B 40 (1979) 291.

[4.27] B. Drevillon and F. Vaillant, Thin Solid Films **124** (1985) 217.

[4.28] J. Tauc, " Amorphous and Liquid Semiconductors ", (Plenum, New York, 1974) p.159.

[4.29] I. Sakata, Y. Hayashi, M. Yamanaka, and H. Karasawa, J. Appl. Phys. **52** (1981) 4334.

[4.30] E.A. Davis and N.F. Mott, Philos. Mag. **22** (1970) 903.

[4.31] T.D. Moustakes, Sol. Energy Mater. **8** (1982) 187.

[4.32] T.V. Herak, *Relation of Optical Properties to Structure and a Multilayer Model for Hydrogenated Silicon,* Ph.D Thesis, University of Manitoba, 1987.

[4.33] E.C. Freeman and W. Paul, Phys. Rev. B **20** (1979) 716.

[4.34] Zhang Fang-qing, Chen Guang-hua, Liu Zhi, and Wang Hui-sheng, J. Non-Cryst. Solids **59** & **60** (1983) 565.

CHAPTER V
CONCLUSIONS

An overview on the structural, optical and electrical properties of a-Si:H thin films has been presented. Effects of substrates bias on the properties of a-Si:H thin films fabricated by ECR microwave plasma CVD have been studied. On the basis of the experimental results, the following conclusions are drawn.

For the table samples with conducting substrates and with their surfaces normal to the dc magnetic field during fabrication, some ion bombardment on the growing film is responsible for the densification of the films and the reduction of dihydrides. A moderate amount of ions arriving on the film surface also tends to increase the deposition rate and to improve both the optical and the electrical properties of the films.

For the floor samples with insulating substrates and with their surfaces parallel to the magnetic field during fabrication, some electron flow to the growing films has a favourable effect on the structural homogeneity because it enhances adatom surface mobility through surface heating. This electron flow is also responsible for the improvement of both the optical and the electrical properties of the films.

Both table and floor samples exhibit a higher density and a better quality when the substrate is biased with - 100 V during fabrication.

Since our conclusions are based on a limited amount of experimental results, further studies are necessary in order to understand the relative roles of ions and electrons during film growth.

Extensive studies on plasma chemistry as well as plasma physics are very important for the further development of the ECR microwave plasma fabrication techniques.